Chemical Papers
https://doi.org/10.1007/s11696-023-02910-4

ORIGINAL PAPER

Comparative study of interaction energies between $\alpha_{IIb}\beta_3$ integrin and the peptidic, peptidomimetic and non-peptidic ligands by quantum mechanics FMO-PIEDA calculations

Juraj Kóňa[1,2]

Received: 23 March 2023 / Accepted: 31 May 2023

Abstract
Integrins belong to a family of cell adhesion receptors. To better understand an adhesion mechanism of integrins, fragmented molecular orbital (FMO) method with pair interaction energy decomposition analysis (PIEDA) was applied for integrin:ligand complexes. Interaction energies were evaluated between the amino acid residues including Mg^{2+} and Ca^{2+} ions at ligand-binding site of $\alpha_{IIb}\beta_3$ integrin and two peptide chains with the Ala-Gly-Asp (AGD)- and the Arg-Gly-Asp (RGD)-binding motifs, a cyclic peptide (eptifibatide), peptidomimetic ligands (tirofiban and L-739758) and poly(L-lactic acid) chain (PLA). The results indicate that Mg^{2+} and Ca^{2+} ions together with Asp224A, Asn215B, Asp159A and Lys125B of $\alpha_{IIb}\beta_3$ are the most important residues for a binding of the peptidic ligands while for the peptidomimetic ligands and PLA, interactions with Ca^{2+} ions are less significant than those with amino acid residues of $\alpha_{IIb}\beta_3$. For all complexes, a dominant part of interaction energy comes from electrostatic interactions. New developed antagonists of $\alpha_{IIb}\beta_3$ should mimic not only the interactions of the RGD motif but also the interactions of the backbone of a longer peptidic sequence (RGDV or AGDV) with the focus on the interactions of the antagonists with the ADMIDAS Ca^{2+} ion. An interaction pattern predicted for PLA was compared with the native peptidic ligands.

Keywords Integrins · Binding mechanism · Polylactic acid · QM/MM calculations · FMO-PIEDA analysis

Introduction

Integrins, selectins, cadherins, immunoglobulins and mucins belong to adhesion molecules (Harjunpää et al. 2019; Chothia and Jones 1997; Tvaroška et al. 2023). Integrins are heterodimeric molecules containing an α and a β subunit (Humphries 2000; Hynes 2002; Campbell and Humphries 2011) with large extracellular domains and short cytoplasmic domains (Springer and Wang 2004; Arnaout et al. 2005). |The ligand-binding site is formed in an interface between the α subunit and the β subunit (Fig. 1). Most integrins bind a wide variety of ligands (Humphries et al. 2006; Zheng and Leftheris 2020). The low affinity state-bent conformation of the integrins can change to the open active conformation forming the ligand-binding site in the β I domain (Luo et al. 2007; Zhu et al. 2013; Xiao et al. 2004). The β I domain has three metal ion-binding sites, with a Mg^{2+} ion in the central metal ion-dependent adhesion site (MIDAS) flanked by two Ca^{2+} ions, one of which is in a site termed adjacent to MIDAS (ADMIDAS). The other Ca^{2+} ion is in a site termed as the ligand-associated metal ion-binding site (LIMBS) (Fig. 1).

Molecular dynamics (MD) simulations of integrins' conformational dynamics were reviewed recently (Tvaroška et al. 2023). The prevailing MD simulations have focused on understanding activation and transition from bent to extended conformations initiated by inside-out and outside-in signaling (Murcia et al. 2008; Puklin-Faucher and Vogel 2009; Ghitti et al. 2012; Craig et al. 2004; Mehrbod et al. 2013; Bidone et al. 2019; Gaillard et al. 2009; Chen et al. 2011; Puklin-Faucher et al. 2006; Wang et al. 2017). Recently, molecular dynamics simulations to the bidirectional adhesion signaling pathway of integrin $\alpha_V\beta_3$ were

✉ Juraj Kóňa
chemkona@savba.sk

[1] Medical Vision, Civic Research Association, Záhradnícka 4837/55, 82108 Bratislava, Slovakia

[2] Institute of Chemistry, Center for Glycomics, Slovak Academy of Sciences, Dúbravska cesta 9, 845 38 Bratislava, Slovakia

Published online: 10 June 2023

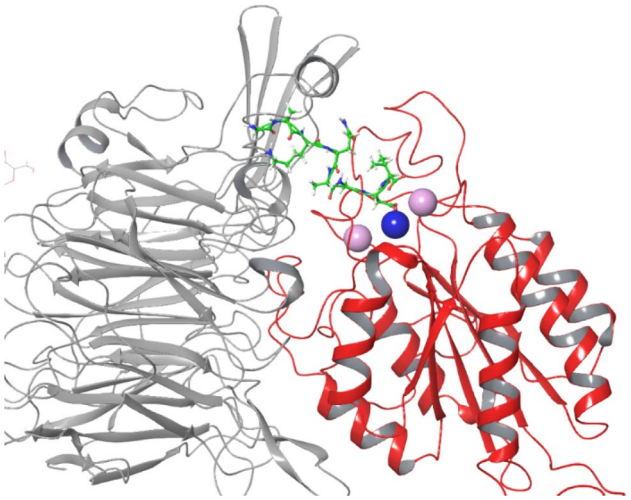

Fig. 1 A 3-D structure of $\alpha_{IIb}\beta_3$ integrin with a bound peptide (with the AGD motif, green). The β subunit β3 I domain (red) has three metal ion-binding sites, with a Mg^{2+} ion (blue ball) flanked by two Ca^{2+} ions (pink balls). The α subunit β-propeller domain is depicted in a gray color

performed (Kulke and Langel 2020). From the results, the most likely mechanism for inside-out and outside-in signaling is the switchblade model with further separation of the transmembrane helices.

Integrins recognize protein ligands through Arg-Gly-Asp (RGD) sequence in flexible loop regions (Springer et al. 2008). However, the adhesion mechanism by which integrins differentiate among proteins with RGD motifs is not well understood (Dong et al. 2014). Based on available X-ray structures of RGD-binding integrins (Xiong et al. 2002; Springer et al. 2008; Dong et al. 2014; Zhu et al. 2008, 2010; Zheng and Leftheris 2020), a negatively charged carboxylate side chain of Asp directly coordinates with the MIDAS Mg^{2+} ion and a positively charged side chain of Arg interacts with Asp residue of the integrin. Other amino acid residues of the protein ligand seems to play an important role for specific binding of the ligand since short peptides with different amino acid sequences with the RGD motif were not always effective antagonist for some studied RGD-binding integrins (Kapp et al. 2017; Kloczewiak et al. 1989). Additionally, isoDGR was found as a new natural recognition motif of the RGD-binding pocket of $\alpha_v\beta_3$ integrin (Spitaleri et al. 2008, 2011). Molecular dynamics simulations revealed that isoDGR-containing cyclopeptides are true $\alpha_v\beta_3$ antagonists which block integrin activation (Ghitti et al. 2012).

Fibrinogen binds to integrin $\alpha_{IIb}\beta_3$ on platelets during hemostasis and thrombosis and both proteins are mentioned in connection with cardiovascular and autoimmune diseases (Huang et al. 2019). $\alpha_{IIb}\beta_3$ integrin also plays a role in cancer progression. $\alpha_{IIb}\beta_3$ binds to RGD-lacking C-terminal region [the AKQAGDV sequence with an Ala-Gly-Asp (AGD) motif] of the γ subunit of fibrinogen (Yang et al. 2001) (Fig. 1). On the other hand, $\alpha_v\beta_3$ integrin binds fibrinogen via a non-terminal RGD motif in fibrinogen's α subunit. As was found by X-ray study (Springer et al. 2008), $\alpha_{IIb}\beta_3$ integrin also bound to a lamprey terminal AKQRGDV sequence with the RGD motif. Therefore, development of selective antagonists of $\alpha_{IIb}\beta_3$ and the closely related $\alpha_V\beta_3$ integrin was efforted in past decades (Xiao et al. 2004).

To compare an interaction pattern between $\alpha_{IIb}\beta_3$ integrin and the peptides with these two motifs, and better understand chemical nature of a complex ligand-binding site of $\alpha_{IIb}\beta_3$ consisted of the three metal ions, quantum mechanics calculations were performed in this study using the two-body fragmented molecular orbital (FMO) method (Kitaura et al. 1999; Fedorov and Kitaura 2009; Fedorov et al. 2012). Due to available X-ray structures (Springer et al. 2008; Xiao et al. 2004), the calculations were also performed for $\alpha_{IIb}\beta_3$ complexes with peptidomimetic antagonists (eptifibatide, tirofiban and L-739758 ligand) (Fig. 2). Eptifibatide is a cyclic L-peptide with the homoarginine-Gly-Asp sequence, and together with tirofiban, they are used in treatment of thrombosis. Both eptifibatide ($IC_{50} = 2.44$ nM) and tirofiban ($IC_{50} = 1.3$ nM) are nanomolar antagonist of $\alpha_{IIb}\beta_3$ (Kapp et al. 2017). L-739758, structurally similar to tirofiban, is an effective antagonist of $\alpha_{IIb}\beta_3$. The FMO-PIEDA calculations for these antagonists of $\alpha_{IIb}\beta_3$ will allow us to compare their interaction patterns with those of native peptidic ligands of $\alpha_{IIb}\beta_3$ and help better to understand their nanomolar biological activities. The calculations will show whether the synthetic antagonists mimic interactions of the native peptidic ligands or interact with $\alpha_{IIb}\beta_3$ specifically. In addition, FMO-PIEDA calculations were also performed for a complex of $\alpha_{IIb}\beta_3$ with a poly(L-lactic acid) (PLA) chain in two conformations (Fig. 3). In one conformation, mimicking terminal C-region of fibrinogen, PLA chains was modeled with its terminal carboxylate coordinated with the MIDAS Mg^{2+} ion, while in the other conformation it interacted with an integrin ligand-binding groove and MIDAS by polyester groups as they were predicted by molecular docking calculations (mimicking the binding of a non-terminal region of a peptidic ligand). PLA is a thermoplastic polyester often used as medical implants in different forms (Suzuki and Ikada 2010). To improve cell adhesion properties of polymers, the integrin-targeting proteins were integrated in different polymeric scaffolds and implant materials (Zhao et al. 2020; Shekaran and García 2011; Kim and Park 2006; Dhavalikar et al. 2020). The FMO-PIEDA calculations for the PLA: $\alpha_{IIb}\beta_3$ complexes will show how well the polyester backbone of PLA mimics the interactions of the peptidic ligands of $\alpha_{IIb}\beta_3$ and which modifications of the structure of PLA could improve its adhesion properties for binging to integrins.

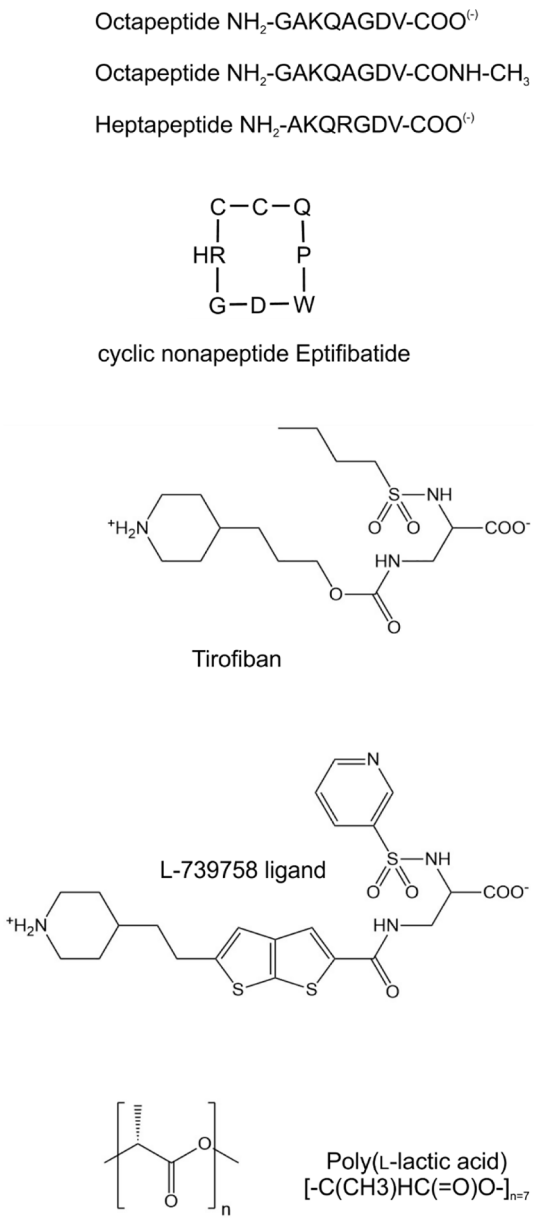

Fig. 2 Structures of ligands used for FMO-PIEDA calculations. Protonation forms of carboxylate and amino groups, as used in the calculations, are shown

Results and discussion

$\alpha_{IIb}\beta_3$:peptide(GAKQAGDV). The complex of the integrin($\alpha_{IIb}\beta_3$):peptide (GAKQAGDV) was used in this study as a template structure for comparison of $\Delta E_{int(L:R)}$ with other complexes. The geometry of an X-ray structure (PDB ID: 2VDP) (Springer et al. 2007b) was firstly optimized at the DFT-QM/MM level. Then the FMO-PIEDA calculations were performed at both DFT (wB97X-D) and ab initio MP2 levels (Tables 1 and 2). Firstly, we wanted to understand which amino acid residues of $\alpha_{IIb}\beta_3$ are most important for binding a native peptide with the AGD motif (Table 1). Then, we also wanted to see which amino acid residues of the peptide (the GAKQAGDV sequence) are the most important for the binding (Table 2). The FMO-PIEDA results of this complex are compiled in Fig. 4 and only results calculated at the MP2/6-31G(d) level are discussed. (The results calculated at the DFT-wB97X-D/6-31G(d) gave similar energy trends and are also given in Tables 1 and 2.) The calculations have revealed that the most significant interactions are between the peptide ligand and the Mg^{2+} ion ($\Delta E_{L:Mg}{}^{2+} = -350.2$ kcal mol^{-1}), the Ca^{2+} ion (ADMIDAS) ($\Delta E_{L:Ca(ADMIDAS)}{}^{2+} = -158.9$ kcal mol^{-1}), the Asp224A ($\Delta E_{L:Asp224A} = -90.5$ kcal mol^{-1}), the Ca^{2+}(LIMBS) ion ($\Delta E_{L:Ca(LIMBS)}{}^{2+} = -75.8$ kcal mol^{-1}), the Asn215B ($\Delta E_{L:Asn215B} = -55.3$ kcal mol^{-1}), the Asp159A ($\Delta E_{L:Asp159A} = -52.1$ kcal mol^{-1}), the Lys125B ($\Delta E_{L:Lys125B} = -49.2$ kcal mol^{-1}) and the Arg214B ($\Delta E_{L:Arg214B} = -43.7$ kcal mol^{-1}). Thus, the most important interactions come from charged fragments of the integrin except for Asn215B. On the other hand, most severe repulsions come from negatively charged amino acid residues, namely Glu220B, Asp251B and Asp119B. These amino acid residues are directly coordinated with Mg^{2+} and both Ca^{2+} ions, and in the FMO calculations, they were modeled as the separate fragments. Thus, their predicted high repulsion with the peptide ligand is supposed to be overestimated, and in real chemical microenvironment, their negative charges are stabilized by coordination with the highly positive Mg^{2+} and Ca^{2+} ions, and the repulsion with the ligand is decreased. The FMO-PIEDA analysis (Table S1 of ESI) of energy terms (ΔE_{els}, ΔE_{exch}, ΔE_{ct+mix}, ΔE_{disp}) of $\Delta E_{L:R\text{-}AA}$ confirmed this trend where the electrostatic energy term, ΔE_{els}, was the most significant part of the interaction energy. To understand which amino acid residues of the peptide are the most important for the binding to $\alpha_{IIb}\beta_3$, the FMO-PIEDA analysis was also evaluated for every amino acid of the GAKQAGDV sequence (Table 2). $\Delta E_{L\text{-}AA:R}$ energies between $\alpha_{IIb}\beta_3$ and the residues of the bound peptide decrease (weaken) in order: Asp410 (-251.8 kcal mol^{-1}) > Lys406 (-193.5 kcal mol^{-1}) > Val411 (-92.8 kcal mol^{-1}) > Gln407 (-62.1 kcal mol^{-1}) > Gly409 (-48.0 kcal mol^{-1}) > Ala408 (-20.0 kcal mol^{-1}) > Gly404 (-5.3 kcal mol^{-1}) > Ala405 (4.0 kcal mol^{-1}). The three most significant residues (Asp410, Val411 and Lys406) interact with the MIDAS Mg^{2+} ion (Asp410, $\Delta E_{L\text{-}Asp410:Mg}{}^{2+} = -301.7$ kcal mol^{-1}), with the ADMIDAS Ca^{2+} ion (Val411, $\Delta E_{L\text{-}Val411:Ca(ADMIDAS)}{}^{2+} = -107.7$ kcal mol^{-1}) and with Asp224A (Lys406, $\Delta E_{L\text{-}Lys406:R\text{-}Asp224A} = -127.9$ kcal mol^{-1}). Val411 is the C-terminal residue terminated with negatively charged carboxylate. Thus, on both sides, on the integrin [Mg^{2+}(MIDAS), Ca^{2+}(ADMIDAS) and Asp224A] and on the peptide (Asp410, Val411 and Lys406), the highly polar amino acid residues and the metal ions seem to play

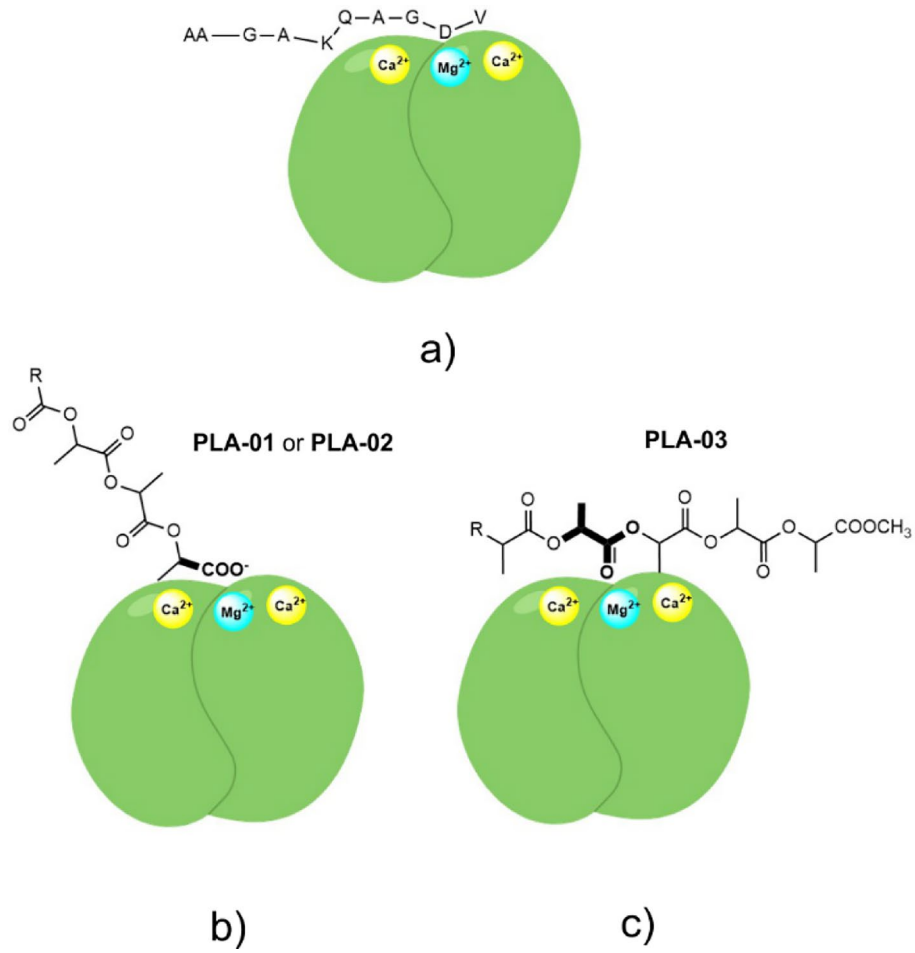

Fig. 3 **a** Schematic representation of interactions between $\alpha_{IIb}\beta_3$ integrin (green) and the peptide with the AGD motif; **b** and PLA interacted via terminal carboxylate with Mg^{2+} ion bound at the MIDAS site (PLA-01 or PLA-02 models); **c** and PLA interacted via backbone polyester groups (PLA-03 model) with the MIDAS, ADMIDAS and LIMBS sites

the most important role for a strong binding of the ligand. The importance of the terminal carboxylate of Val411 for the binding was also confirmed by additional FMO-PIEDA calculations where in C-terminal Val411 of the bound peptide the charged carboxylate (GAKQAGDV-COO^-) was substituted by *N*-methyl amido group (GAKQAGDV-CONH-CH_3). In such peptide, interaction energy for Val411-CONH-CH_3 fragment was decreased to − 6.5 kcal mol^{-1} (from − 92.8 kcal mol^{-1} found in GAKQAGDV-COO^-, $\Delta E_{Val411:R}$). One of the reasons may be a repulsion between the Val411-CONH-CH_3 and the ADMIDAS Ca^{2+} ion ($\Delta E_{Val411:Ca(ADMIDAS)}{}^{2+}$ = 20.4 kcal mol^{-1}), which on the other hand is the major contributor of the interaction energy for the peptide with Val411-COO^- ($\Delta E_{Val411:Ca(ADMIDAS)}{}^{2+}$ = − 107.7 kcal mol^{-1}). Indeed, the importance of the free carboxylate group of the C-terminal residue Val411 for an interaction with the ADMIDAS Ca^{2+} ion was demonstrated by experiments where γC peptides with the carboxylate substituted by amide blocked fibrinogen binding to $\alpha_{IIb}\beta_3$ (Kloczewiak et al. 1989). Moreover, a substitution of Val411 by cysteine, tyrosine or leucine led to a dramatic decreasing of the binding properties of the ligand, while the substitution with phenylalanine maintained the activity of γC peptides (Kloczewiak et al. 1989; Kapp et al. 2017). We conclude that the interaction of $\alpha_{IIb}\beta_3$ with the backbone of Val411 is more significant compared with its side chain. In case of the substitution with cysteine, tyrosine or leucine, the structure of their side chains may be more important for a tight binding to the ADMIDAS Ca^{2+} ion and subsequent strong interactions of their backbones with $\alpha_{IIb}\beta_3$ and the ADMIDAS Ca^{2+} ion itself.

The bound peptide does not directly coordinate with the ADMIDAS Ca^{2+} ion and interacts (via terminal carboxylate of Val411) with it via a water molecule [Peptide-Val411-COO^-–H_2O(254)–Ca^{2+}(ADMIDAS), Fig. 4]. To see a role of the water molecule for the binding of the peptide, $\Delta E_{L:H2O(254)}$ and $\Delta E_{Ca(ADMIDAS):H2O(254)}$ were also analyzed. Both FMO-PIEDA interaction energies ($\Delta E_{L:H2O(254)}$ = − 37.3 kcal mol^{-1} and $\Delta E_{Ca(ADMIDAS):H2O(254)}$ = − 35.8 kcal mol^{-1}) are with significant values; thus, they are significant contributors to a total interaction energy between the peptide and the ADMIDAS Ca^{2+} ion ($\Delta E_{L:Ca(ADMIDAS)}{}^{2+}$ = − 158.9 kcal m ol^{-1}, Table 1). Similarly as it was for the ADMIDAS Ca^{2+} ion, the LIMBS Ca^{2+} ion is not in a direct contact with the bound ligand. Despite the larger distance between the

Table 1 Calculated total interaction energies ($\Delta E_{int(L:R)}$, in kcal mol^{-1}) between the bound ligand (L) and $\alpha_{IIb}\beta_3$ (Receptor, R) at the ab initio MP2/6-31G(d) and DFT-wB97X-D/6-31G(d) (in parentheses) levels

$\Delta E_{int(L:R)} = \Delta E_{L:Mg^{2+}} + \Delta E_{L:Ca^{2+}(ADMIDAS)} + \Delta E_{L:Ca^{2+}(LIMBS)} + \Delta E_{L:R\text{-}Asp224A} + \Delta E_{L:R\text{-}Asp159A} + \Delta E_{L:R\text{-}Asn215B} + \Delta E_{L:R\text{-}Lys125B} + \Delta E_{L:R\text{-}X}$

Ligand	$\Delta E_{int(L:R)}$	$\Delta E_{L:Mg^{2+}}$ MIDAS	$\Delta E_{L:Ca^{2+}}$ ADMIDAS	$\Delta E_{L:Ca^{2+}}$ LIMBS	$\Delta E_{L:R\text{-}Asp224A}$	$\Delta E_{L:R\text{-}Asp159A}$	$\Delta E_{L:R\text{-}Asn215B}$	$\Delta E_{L:R\text{-}Lys125B}$	$\Delta E_{L:R\text{-}X}$
GAKQAGDV-COO$^-$	−708.6 (−702.3)	−350.3 (−343.5)	−158.9 (−185.1)	−75.8 (−108.9)	−90.5 (−88.6)	−52.1 (−50.1)	−55.3 (−53.3)	−49.2 (−47.3)	123.5 (174.5)
GAKQAGDV-CONCH$_3$	−618.8 (−675.5)	−275.1 (−268.8)	−39.2 (−68.9)	−29.9 (−63.3)	−105.3 (−103.0)	−69.2 (−66.7)	−47.0 (−45.1)	−22.1 (−20.9)	−31.0 (−38.8)
AKQRGDV-COO$^-$	−736.0 (−795.7)	−352.0 (−346.3)	−169.4 (−196.1)	−75.6 (−109.2)	−63.7 (−62.4)	−25.7 (−27.4)	−52.6 (−50.4)	−49.2 (−47.4)	52.2 (43.5)
Eptifibatide	−505.6 (−524.0)	−265.2 (−261.6)	3.2 (−33.4)	−42.3 (−55.7)	−103.1 (−105.1)	−17.0 (−67.4)	−37.7 (−44.9)	−19.6 (−20.9)	23.9 (−65.0)
Tirofiban	–415.6 (−419.5)	−248.4 (−242.9)	−51.3 (−51.3)	−34.8 (−48.8)	−99.2 (−96.1)	−11.5 (−11.0)	−36.9 (−34.9)	−21.8 (−21.1)	88.3 (86.6)
L − 739758	−482.7 (−422.7)	−265.5 (−249.1)	−56.4 (−48.5)	−27.5 (−44.3)	−112.0 (−110.9)	−33.7 (−35.1)	−36.5 (−31.9)	−23.7 (−19.8)	72.6 (116.9)
					$\Delta E_{L:R\text{-}Tyr122B}$	$\Delta E_{L:R\text{-}Lys125B}$	$\Delta E_{L:R\text{-}Asn215B}$	$\Delta E_{L:R\text{-}Lys125B}$	
PLA-01	−266.2 (−265.4)	−290.7 (−282.7)	−46.8 (−76.3)	−43.6 (−75.5)	−22.4 (−17.8)	−25.8 (−25.1)	−41.4 (−43.7)	−25.8 (−25.1)	230.3 (280.8)
PLA-02	−272.1 (−259.9)	−292.0 (−284.9)	−73.7 (−72.8)	−60.3 (−91.2)	−21.3 (−20.4)	−28.7 (−27.7)	−43.0 (−41.1)	−28.8 (−27.8)	275.7 (306.0)
					$\Delta E_{L:R\text{-}Asp224A}$	$\Delta E_{L:R\text{-}Asp159A}$	$\Delta E_{L:R\text{-}Arg214B}$	$\Delta E_{L:R\text{-}Asp217B}$	
PLA-03	−127.1 (−137.2)	−15.24 (−14.7)	−1.0 (−1.2)	6.24 (5.4)	−17.1 (−16.6)	−20.1 (−19.4)	−14.0 (−15.2)	−14.0 (−12.9)	−51.9 (−62.6)

Also interaction energies ($\Delta E_{L:Mg^{2+}}$, $\Delta E_{L:Ca(ADMIDAS)^{2+}}$ and $\Delta E_{L:Ca(LIMBS)^{2+}}$) between the ligand and the MIDAS (Mg^{2+}), the ADMIDAS (Ca^{2+}), the LIMBS (Ca^{2+}) ions and other amino acid residues of the integrin with significant $\Delta E_{L:R\text{-}AA}$ are also compiled. $\Delta E_{L:R\text{-}X}$ presents interaction energy between the ligand and the remainder of amino acid fragments of the receptor

Table 2 Interaction energies ($\Delta E_{L\text{-}AA:R}$, in kcal mol^{-1}) between the amino acid residues of the bound peptides (Ligand, L)and $\alpha_{IIb}\beta_3$ integrin (Receptor, R) calculated at the ab initio MP2/6-31G(d) and DFT-wB97X-D/6-31G(d) (in parentheses) levels

Peptides	GAKQAGDV-COO$^-$	GAKQAGDV-CONCH$_3$		AKQRGDV		Eptifibatide
$\Delta E_{L\text{-}G404:R}$	−5.28 (−4.48)	−5.00 (−7.21)	$\Delta E_{L\text{-}G404:R}$		$\Delta E_{L\text{-}G1:R}$	−24.9 (−25.74)
$\Delta E_{L\text{-}A405:R}$	3.96 (4.64)	4.85 (0.69)	$\Delta E_{L\text{-}A405:R}$	−12.66 (−14.04)	$\Delta E_{L\text{-}D2:R}$	−202.89 (−227.08)
$\Delta E_{L\text{-}K406:R}$	−193.49 (−183.09)	−205.56 (−208.13)	$\Delta E_{L\text{-}K406:R}$	−33.33 (−35.12)	$\Delta E_{L\text{-}W3:R}$	44.74 (−24.96)
$\Delta E_{L\text{-}Q407:R}$	−62.10 (−54.62)	−61.99 (−58.48)	$\Delta E_{L\text{-}Q407:R}$	−50.44 (−52.57)	$\Delta E_{L\text{-}P4:R}$	−3.98 (−33.43)
$\Delta E_{L\text{-}A408:R}$	−20.01 (−17.54)	−21.08 (−23.76)	$\Delta E_{L\text{-}R408:R}$	−183.66 (−189.14)	$\Delta E_{L\text{-}C5:R}$	14.46 (−23.64)
$\Delta E_{L\text{-}G409:R}$	−48.03 (−43.72)	−50.00 (−49.18)	$\Delta E_{L\text{-}G409:R}$	−44.88 (−45.06)	$\Delta E_{L\text{-}HR6:R}$	−198.81 (−200.3)
$\Delta E_{L\text{-}D410:R}$	−251.75 (−262.13)	−234.96 (−255.36)	$\Delta E_{L\text{-}D410:R}$	−246.71 (−269.17)		
$\Delta E_{L\text{-}V411:R}$	−92.83 (−144.74)	−6.46 (−74.13)	$\Delta E_{L\text{-}V411:R}$	−127.13 (−183.3)		

ligand and the Ca^{2+} ions (> 4.5 Å), their interactions were significant. The PIEDA analysis (Table S1 of ESI) showed that the main contributor to total interaction energy between the ligand and the Ca^{2+} ions is the electrostatic energy term ($\Delta E^{els}{}_{L:Ca(ADMIDAS)^{2+}} = -202.5$ kcal mol^{-1} of $\Delta E_{L:Ca(ADMIDAS)^{2+}} = -158.9$ kcal mol^{-1}; and $\Delta E^{els}{}_{L:Ca(LIMBS)^{2+}} = -116.7$ kcal mol^{-1} of $\Delta E_{L:Ca(ADMIDAS)^{2+}} = -75.8$ kcal mol^{-1}).

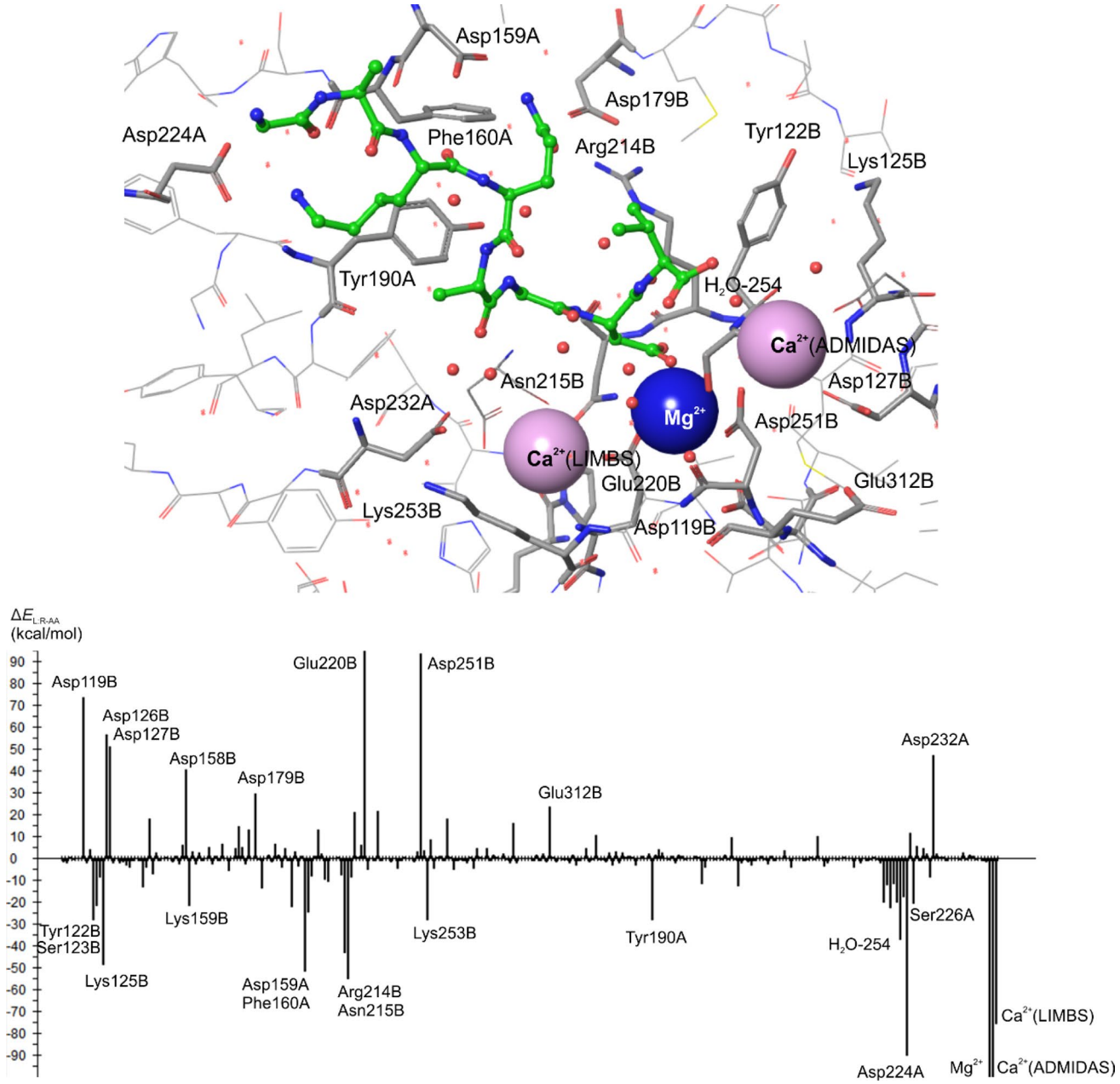

Fig. 4 FMO-PIEDA interaction energies ($\Delta E_{\text{L:R-AA}}$, in kcal mol^{-1}) between the peptide with the AGD motif (GAKQAGDV-COO$^-$) and the amino acid residues of $\alpha_{\text{IIb}}\beta_3$ calculated at the ab initio MP2/6-31G(d) level. The attraction terms of $\Delta E_{\text{int(L:R)}}$ present $\Delta E_{\text{L:R-AA}}$ with the negative values, while repulsion terms are with the positive values. The amino acid residues with the most significant $\Delta E_{\text{L:R-AA}}$ are visualized (tube representation, gray) as well as the bound peptide (ball-and-stick representation, green)

The AGD motif of the native ligand of $\alpha_{\text{IIb}}\beta_3$ contains the glycine residue. Glycin does not contain a side chain and may be most flexible part of the backbone of the peptides and proteins. Thus, it is important in conformational changes and folding in proteins. Here in the peptide:$\alpha_{\text{IIb}}\beta_3$ complex, Gly409 of the peptidic ligand, seems also to play an important role for the binding. Its interaction energy with $\alpha_{\text{IIb}}\beta_3$ was predicted with a significant value of − 48.0 kcal mol^{-1} ($\Delta E_{\text{Gly409:R}}$, Table 2). It should be noted that a FMO fragmentation technique with the shifted backbone definition was used in this study (Sladek and Fedorov 2022). It means that the Gly409 fragment includes the amide bond consisted of amine group of Gly409 and carbonyl group of Ala408. Detailed analysis of the FMO results showed that this backbone amide bond (Ala408-Gly409) interacts with Ala218B ($\Delta E_{\text{L-Gly409:R-Ala218B}} = -$ 8.5 kcal mol^{-1}), three water molecules, two of them via carbonyl oxygen ($\Delta E_{\text{L-Gly409:H2O(201)}} = -$ 13.9 kcal mo

l^{-1}, $\Delta E_{\text{L-Gly409:H2O(257)}} = -14.5$ kcal mol^{-1}) and one via amide group ($\Delta E_{\text{L-Gly409:H2O(258)}} = -9.5$ kcal mol^{-1}) and the LIMBS Ca^{2+} ion ($\Delta E_{\text{L-Gly409:Ca(LIMBS)}} = -7.5$ kcal mo l^{-1}). Similarly, as it was for Val411 of the peptidic ligand, the interaction of the Ala408-Gly409 backbone with $\alpha_{IIb}\beta_3$ seem to play an important role for the binding of the peptide with the AGD motif.

$\alpha_{IIb}\beta_3$:AKQRGDV peptide. Whereas ligands with the RGD motif binds to eight different integrins, the fibrinogen γC peptide with the AGD motif binds only to $\alpha_{IIb}\beta_3$. In contrast, the A408R mutation of the native γC peptide, which produced the RGD motif, did bind to $\alpha_{IIb}\beta_3$ (Springer et al. 2008). In the X-ray structure (PDB ID: 2VDR) (Springer et al. 2007a), this arginine substitute a 3-D position of Lys406 and interacts with Asp224A of $\alpha_{IIb}\beta_3$, while Lys406 interacts with Asp159A of $\alpha_{IIb}\beta_3$. We calculated a FMO-PIEDA energy profile for the $\alpha_{IIb}\beta_3$:peptide complex to see how presence of Arg408 and 3-D reorganization of the peptide change interactions with the integrin. The FMO-PIEDA results for every amino acid of the AKQRGDV sequence of the peptide are compile in Table 2, and for the most important amino acid residues of $\alpha_{IIb}\beta_3$, the results are in Table 1. $\Delta E_{\text{L-AA:R}}$ between the residues of the peptide and $\alpha_{IIb}\beta_3$ integrin decreases (weakens) in the following order: Asp410 (− 246.7 kcal mol^{-1}) > Arg408 (− 183.7 kcal mol^{-1}) > Val411 (− 127.13 kcal mol^{-1}) > Gln407 (− 50.4 kcal mol^{-1}) > Gly409 (− 44.9 kcal mol^{-1}) > Lys406 (− 33.3 kcal mol^{-1}) > Ala405 (− 12.7 kcal mol^{-1}). Thus, the order of significance is almost the same, as for the native peptide with the AGD motif, with an exception of Arg408, which now is a better contributor to total $\Delta E_{\text{int(L:R)}}$ as Val411 and Lys406 (Figure S1 of ESI). Again, as it was for the peptide with the AGD motif, the three most significant residues (Asp410, Arg408 and Val411) interact with the MIDAS Mg^{2+} ion (Asp410, $\Delta E_{\text{L-Asp410:Mg}}{}^{2+} = -300.6$ kcal mol^{-1}), with the ADMIDAS Ca^{2+} ion (Val411, $\Delta E_{\text{L-Val411:Ca(ADMIDAS)}}{}^{2+} = -116.0$ kcal mol^{-1}) and with Asp224A (Arg408, $\Delta E_{\text{L-Arg408:R-Asp224A}} = -105.4$ kcal mo l^{-1}). Thus, both the AKQAGDV and AKQRGDV sequences present an optimal 3-D structure for specific binding of γ subunit of fibrinogen to $\alpha_{IIb}\beta_3$. The total $\Delta E_{\text{int(L:R)}}$ for the peptide with the RGD motif is stronger ($\Delta E_{\text{int(L:R)}} = -736.0$ kcal mol^{-1}) compared with that for the peptide with the AGD motif ($\Delta E_{\text{int(L:R)}} = -708.6$ kcal mol^{-1}) (Fig. 5). This supports the finding that the substitution of Ala408 by Arg in human fibrinogen γC chain (dodecapeptide γC 400–411) led to gain 6 times on binding potency (Kloczewiak et al. 1989; Timmons et al. 1989). A similar result was obtained by Ruggeri et al., where the IC_{50} for γC 400–411 was 48–180 μM and only 14.5 μM for the A408R mutant (Ruggeri et al. 1986). Indeed, lamprey and xenopus, in contrast to human, γC sequences of fibrinogen contain the RGD motif (Springer et al. 2008).

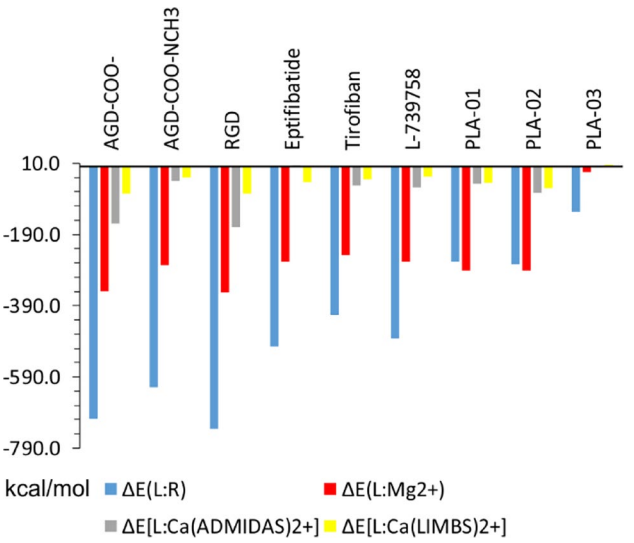

Fig. 5 FMO-PIEDA interaction energies ($\Delta E_{\text{int(L:R)}}$, in kcal mol^{-1}, blue) between the bound ligands and $\alpha_{IIb}\beta_3$ calculated at the ab initio MP2/6-31G (d) level. Also interaction energies ($\Delta E_{\text{L:Mg(MIDAS)}}{}^{2+}$, red; $\Delta E_{\text{L:Ca(ADMIDAS)}}{}^{2+}$, gray; and $\Delta E_{\text{L:Ca(LIMBS)}}{}^{2+}$, yellow) between the ligand and the MIDAS Mg^{2+}, ADMIDAS Ca^{2+} and LIMBS Ca^{2+} ions are also compiled

The most important contributors of $\alpha_{IIb}\beta_3$ to $\Delta E_{\text{int(L:R)}}$ are the MIDAS Mg^{2+} ion ($\Delta E_{\text{L:Mg(MIDAS)}}{}^{2+} = -352.0$ kcal mo l^{-1}), the ADMIDAS Ca^{2+} ion ($\Delta E_{\text{L:Ca(ADMIDAS)}}{}^{2+} = -169.4$ kcal mol^{-1}), Asp224A ($\Delta E_{\text{L:Asp224A}} = -63.7$ kcal mol^{-1}), the LIMBS Ca^{2+} ion ($\Delta E_{\text{L:Ca(LIMBS)}}{}^{2+} = 75.63$ kcal mol^{-1}), Asn215B ($\Delta E_{\text{L:Asn215B}} = -52.6$ kcal mol^{-1}), Asp159A ($\Delta E_{\text{L:Asp159A}} = 25.7$ kcal mol^{-1}), Lys125B ($\Delta E_{\text{L:Lys125B}} = -49.2$ kcal mol^{-1}) and Arg214B ($\Delta E_{\text{L:Arg214B}} = -42.2$ kcal mol^{-1}) (Fig. 6). The detailed PIEDA analysis showed that electrostatic interactions are a dominant part of $\Delta E_{\text{int}}{}_{\text{(L:R)}}$ (Table S2 of ESI).

Complexes $\alpha_{IIb}\beta_3$:peptidomimetic ligands. Based on available X-ray structures (Springer et al. 2008; Springer et al. 2007c, e, d), complexes of $\alpha_{IIb}\beta_3$ with cyclic peptide eptifibatide, nanomolar blocker tirofiban and the L-739758 ligand FMO-PIEDA interaction patterns were calculated (Figs. 7, 8 and 9) and compared with the results of the complexes of $\alpha_{IIb}\beta_3$ with the previously discussed peptides with the AGD and the RGD motifs. For these three ligands, the interactions with the MIDAS Mg^{2+} ion, the ADMIDAS Ca^{2+} ion and the LIMBS Ca^{2+} ion are dominant except for eptifibatide. For this ligand only interactions with the MIDAS Mg^{2+} ion and the LIMBS Ca^{2+} ion are significant [$\Delta E_{\text{L:Mg(MIDAS)}}{}^{2+} = -265.2$ kcal mol^{-1} and $\Delta E_{\text{L:Ca(LIMBS)}}{}^{2+} = -42.3$ kcal mol^{-1}], in opposite, with the ADMIDAS Ca^{2+} ion are repulsive ($\Delta E_{\text{L:Ca(ADMIDAS)}}{}^{2+} = 3.2$ kcal mol^{-1}). The detailed analysis of the PIEDA energy contributors

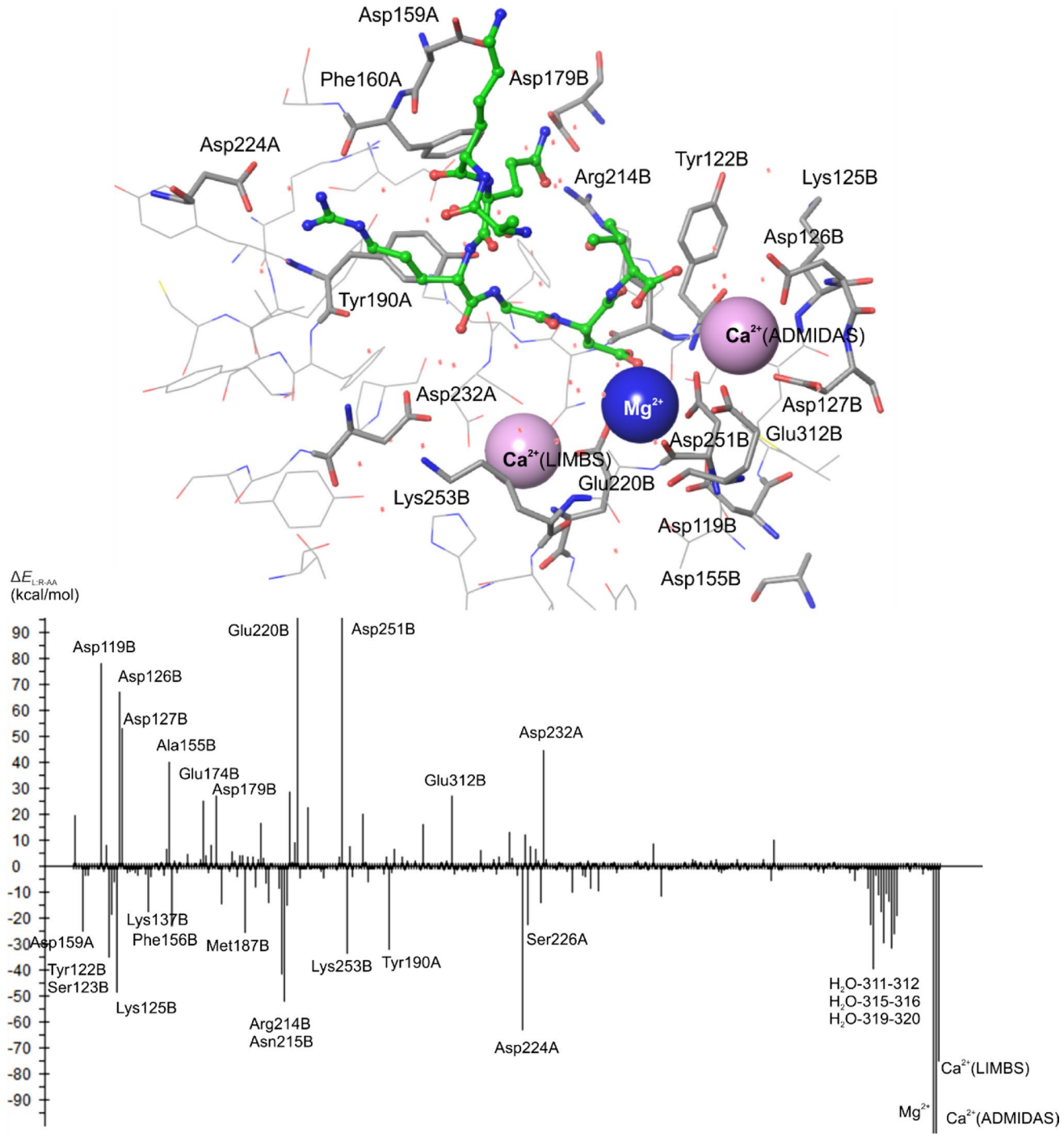

Fig. 6 FMO-PIEDA interaction energies ($\Delta E_{\text{L:R-AA}}$, in kcal mol^{-1}) between the peptide with the RGD motif (AKQRGDV-COO$^-$) and the amino acid residues of $\alpha_{\text{IIb}}\beta_3$ calculated at the ab initio MP2/6-31G(d) level. The attraction terms of $\Delta E_{\text{int(L:R)}}$ present $\Delta E_{\text{L:R-AA}}$ with the negative values, while repulsion terms are with the positive values. The amino acid residues with the most significant $\Delta E_{\text{L:R-AA}}$ are visualized (tube representation, gray) as well as the bound peptide (ball-and-stick representation, green)

has showed that although ${\Delta E^{\text{els}}}_{\text{L:Ca(ADMIDAS)}}{}^{2+}$ is attractive (− 26.1 kcal mol^{-1}), ${\Delta E^{\text{disp}}}_{\text{L:Ca(ADMIDAS)}}{}^{2+}$ is strongly repulsive (31.7 kcal mol^{-1}). This finding is also supported by steered molecular dynamics (SMD) simulations where the ADMIDAS Ca^{2+} ion had the lowest effect on SMD force profiles of the unbinding of eptifibatide from $\alpha_{\text{IIb}}\beta_3$ (Murcia et al. 2008).

Overall, the interactions of the ligands with the MIDAS Mg^{2+} ion calculated in this study are the most significant (Fig. 5). The dominant part of ${\Delta E_{\text{L:Mg}}}^{2+}$ is an electrostatic

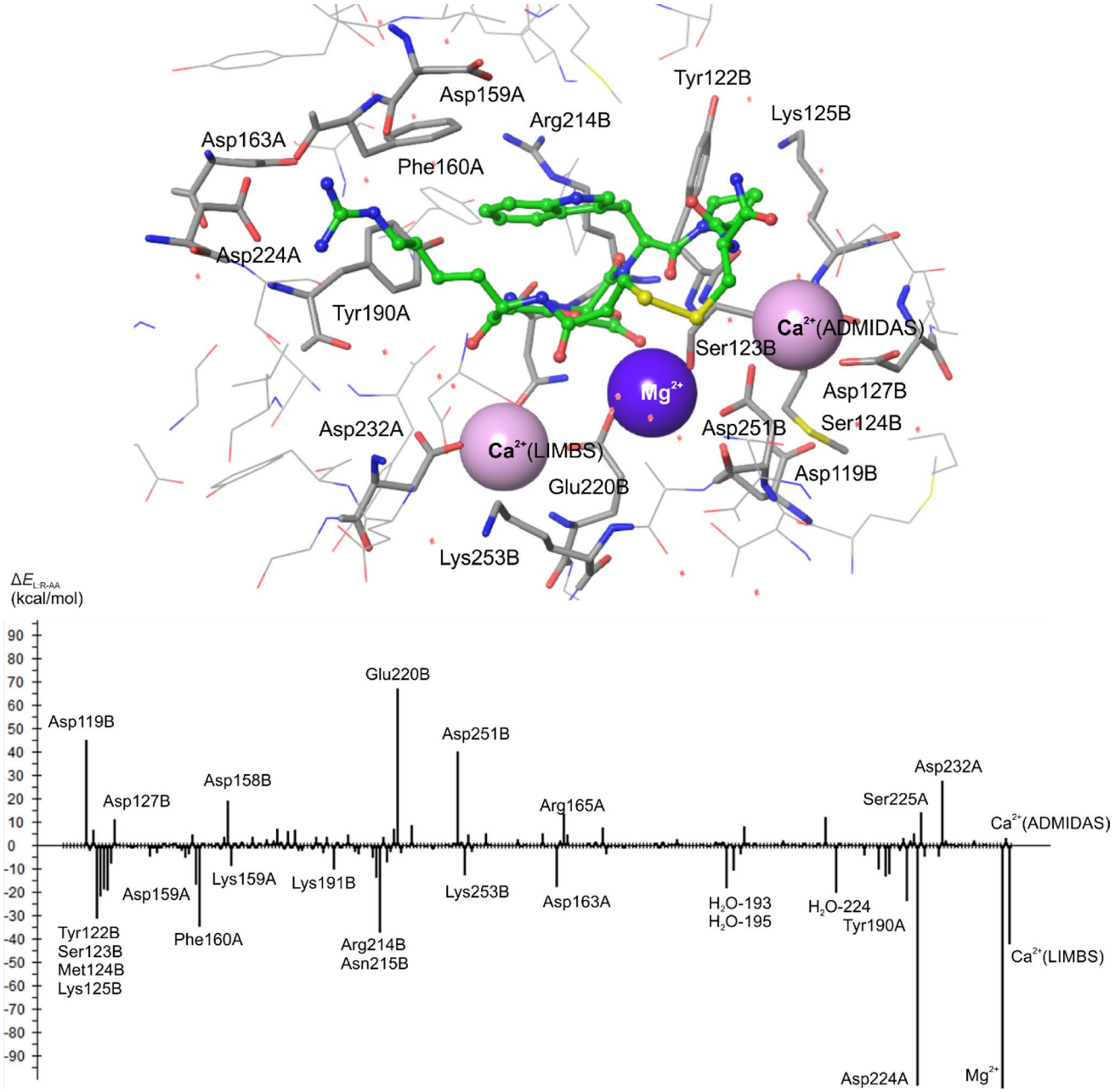

Fig. 7 FMO-PIEDA interaction energies ($\Delta E_{\mathrm{L:R\text{-}AA}}$, in kcal mol^{-1}) between the eptifibatide and the amino acid residues of $\alpha_{\mathrm{IIb}}\beta_3$ calculated at the ab initio MP2/6-31G(d) level. The attraction terms of $\Delta E_{\mathrm{int(L:R)}}$ present $\Delta E_{\mathrm{L:R\text{-}AA}}$ with the negative values, while repulsion terms are with the positive values. The amino acid residues with the most significant $\Delta E_{\mathrm{L:R\text{-}AA}}$ are visualized (tube representation, gray) as well as the bound peptidomimetic ligand (ball-and-stick representation, green)

term ($\Delta E^{\mathrm{els}}{}_{\mathrm{L:Mg(MIDAS)}}{}^{2+} = -254.5$ kcal mol^{-1} of $\Delta E_{\mathrm{L:Mg(MIDAS)}}{}^{2+} = -265.2$ kcal mol^{-1} for eptifibatide; $\Delta E^{\mathrm{els}}{}_{\mathrm{L:Mg(MIDAS)}}{}^{2+} = -235.2$ kcal mol^{-1} of $\Delta E_{\mathrm{L:Mg(MIDAS)}}{}^{2+} = -248.4$ kcal mol^{-1} for tirofiban; and $\Delta E^{\mathrm{els}}{}_{\mathrm{L:Mg(MIDAS)}}{}^{2+} = -250.3$ kcal mol^{-1} of $\Delta E_{\mathrm{L:Mg(MIDAS)}}{}^{2+} = -265.5$ kcal mol^{-1} for the L-739758 ligand). As it was for the peptides, Asp224A, Asn215B, Tyr122B, Lys125B and Tyr190A of $\alpha_{\mathrm{IIb}}\beta_3$ (Table 1, Figs. 6, 7 and 8) are also the most important contributors to total $\Delta E_{\mathrm{int(L:R)}}$ for the $\alpha_{\mathrm{IIb}}\beta_3$ complexes with the peptidomimetic ligands. In conclusion, eptifibatide, tirofiban and the L-739758 ligand interact with $\alpha_{\mathrm{IIb}}\beta_3$ with similar interaction patterns as native peptidic ligands of $\alpha_{\mathrm{IIb}}\beta_3$. These may explain why they bind $\alpha_{\mathrm{IIb}}\beta_3$ at the nanomolar level (Kapp et al. 2017).

Complexes $\alpha_{\mathrm{IIb}}\beta_3$:PLA. The PLA chains with a terminal carboxylate group (the PLA-COO$^-$ configuration) as well

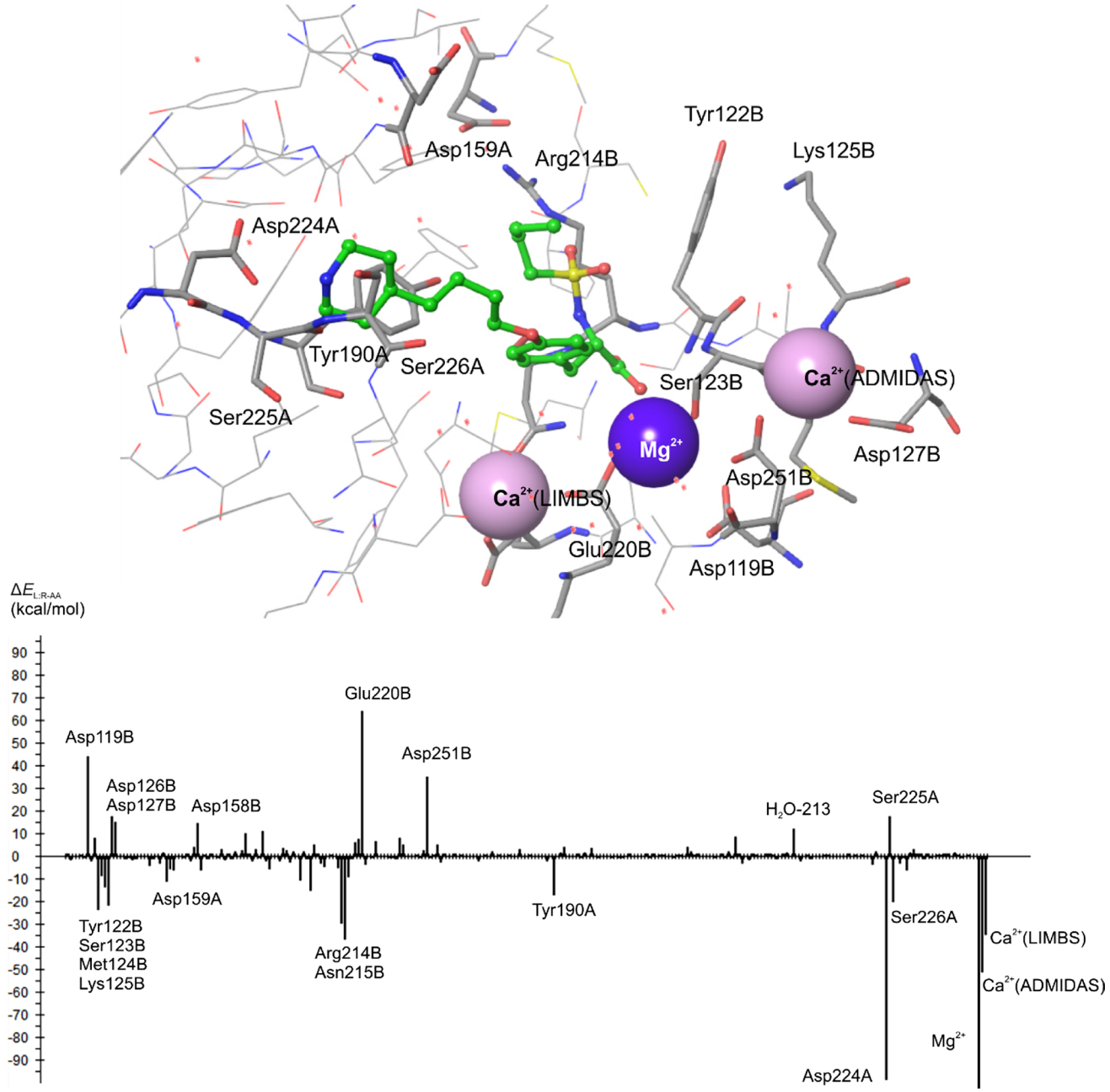

Fig. 8 FMO-PIEDA interaction energies ($\Delta E_{L:R\text{-}AA}$, in kcal mol^{-1}) between the tirofiban and the amino acid residues of $\alpha_{IIb}\beta_3$ calculated at the ab initio MP2/6-31G(d) level. The attraction terms of $\Delta E_{int(L:R)}$ present $\Delta E_{L:R\text{-}AA}$ with the negative values, while repulsion terms are with the positive values. The amino acid residues with the most significant terms of $\Delta E_{L:R\text{-}AA}$ are visualized (tube representation, gray) as well as the bound peptidomimetic ligand (ball-and-stick representation, green)

as with a terminal methyl ester group (the PLA-$COOCH_3$ configuration) were docked into the ligand-binding site of $\alpha_{IIb}\beta_3$. The PLA-COO^- chain was found to bind with terminal carboxylate to the MIDAS Mg^{2+} ion [d(PLA-COO^-:Mg^{2+}) = 2.13 Å] and with the polyester chain bound along a groove flanked by Asp159A, Asp224A and Ser226A on the one side and Arg214B, Tyr122B, Asn215B and the MIDAS Mg^{2+} ion on the other side (Fig. 10, PLA-01 model). PLA-$COOCH_3$ bound in a similar conformation, however, interacting with the MIDAS Mg^{2+} ion [d(PLA-$COOCH_3$:Mg^{2+}) = 3.66 Å] with one of the ester groups at a middle of its chain, and with the terminal methyl ester group positioned at a hydrophobic groove flanked by Val156A and Met180B (Fig. 11, PLA-03 model). This groove was not filled by any conformations with the PLA-COO^- configuration. For the subsequent QM/MM geometry optimizations

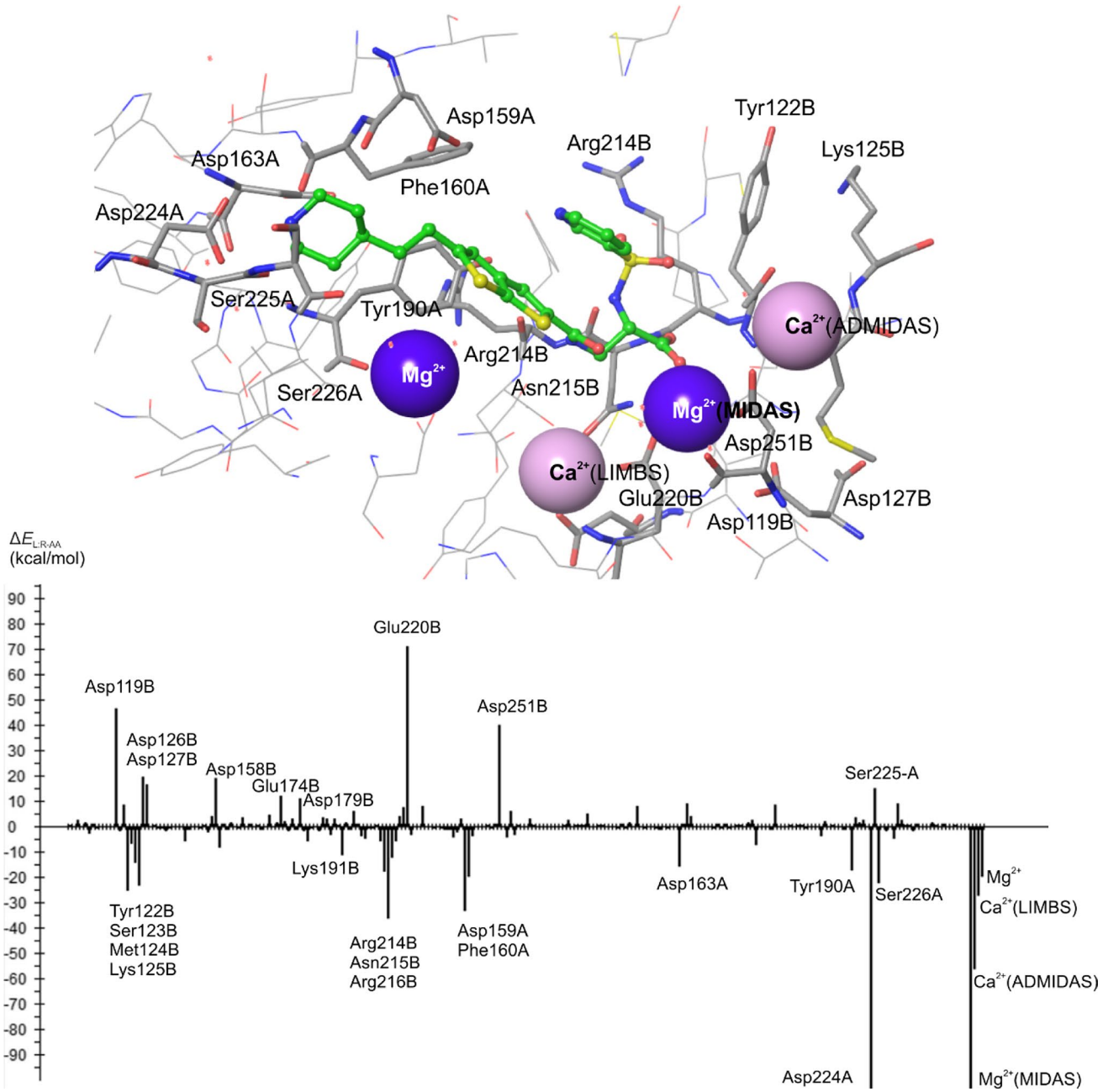

Fig. 9 FMO-PIEDA interaction energies ($\Delta E_{L:R\text{-}AA}$, in kcal mol^{-1}) between the peptidomimetic ligand (L-739758) and the amino acid residues of $\alpha_{IIb}\beta_3$ calculated at the ab initio MP2/6-31G(d) level. The attraction terms of $\Delta E_{int(L:R)}$ present $\Delta E_{L:R\text{-}AA}$ with the negative values, while repulsion terms are with the positive values. The amino acid residues with the most significant $\Delta E_{L:R\text{-}AA}$ are visualized (tube representation, gray) as well as the bound peptidomimetic ligand (ball-and-stick representation, green)

and FMO-PIEDA calculations, two conformations with the best docking scores (PLA-01 and PLA-02) with the PLA-COO^- configuration and one conformation (PLA-03) with PLA-$COOCH_3$ were selected. The FMO-PIEDA results are compiled in Figs. 12, 13 and S3 and Table 1. The total $\Delta E_{int(L:R)}$ for the complexes with the PLA chain was 2–5 times weaker compared with the complexes with the native peptides or peptidomimetic ligands (Fig. 5). For example, $\Delta E_{int(L:R)}$(PLA-01) = − 272.1 kcal mol^{-1} or $\Delta E_{int(L:R)}$(PLA-03) = − 127.1 kcal mol^{-1} *versus* $\Delta E_{int(L:R)}$(GAKQAGDV peptide) = − 708.6 kcal mol^{-1}. One of the reasons for the weakening of the interaction energy is in weaker interactions of the PLA chain with the MIDAS Mg^{2+} ion, the ADMIDAS Ca^{2+} ion and the LIMBS Ca^{2+} ion (Fig. 5). This is mainly evident for the PLA chain without the terminal carboxylate

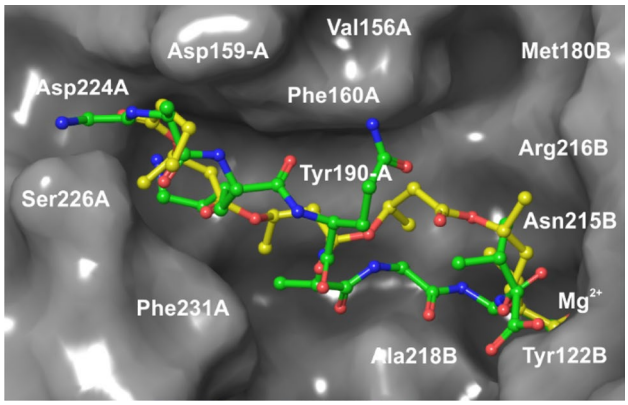

Fig. 10 Superposition of the PLA-01 ligand (yellow) with the peptide (the GAKQAGDV sequence, green) at the ligand-binding site of $\alpha_{IIb}\beta_3$ (QM/MM optimized integrin:ligand complexes)

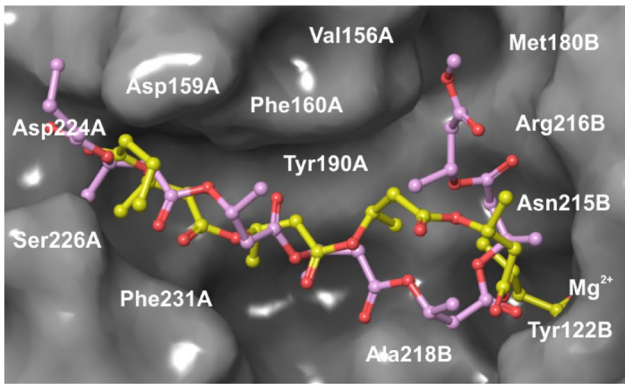

Fig. 11 Superposition of the PLA-01 ((PLA-COO^-, yellow) with the PLA-03 ligand ((PLA-$COOCH_3$, magenta) at the ligand-binding site of $\alpha_{IIb}\beta_3$ (QM/MM optimized ligand:integrin complexes)

group (PLA-03). Therefore, the adhesion of PLA surface on a cell may be more efficient when free carboxylates are available on polymer surfaces in repeated intervals. This conclusion is clearly evident from FMO-PIEDA analysis comparing the PLA-01 (or PLA-02) and PLA-03 interaction patterns (Fig. 12, 13 and S3 of ESI). For PLA-03, key interactions with amino acid residues of $\alpha_{IIb}\beta_3$ (Asp159A, Phe160A, Tyr190A, Arg214B and Asp224A) are diminished compared with those found for the peptides, peptidomimetic antagonist and PLA-01 and PLA-02. This indicates that the ligand-binding site of $\alpha_{IIb}\beta_3$ is structurally design to bind a C-terminal peptide with two negatively charged carboxylate groups positioned close to each other (approximately 6 Å, a distance between carboxylate of Val411 and Asp410 of the native γC peptide), while in PLA-01 (or PLA-02) is only one terminal carboxylate group and in PLA-03 no free carboxylate or a negatively charged group.

Conclusion

The FMO-PIEDA calculations were performed to add, beside available structural and biochemical data, next physicochemical properties of two peptidic, three peptidomimetic ligands and the poly(L-lactic acid) chain bound to $\alpha_{IIb}\beta_3$ integrin. The predicted interaction profiles of the integrin:ligand complexes may be described by several basic features: (i) dominant interactions are electrostatic, including interactions of the ligands with the MIDAS Mg^{2+}, the ADMIDAS Ca^{2+} (except for eptifibatide in which dispersion repulsion was dominant) and the LIMBS Ca^{2+} ions; (ii) all three ions at the ligand-binding site of $\alpha_{IIb}\beta_3$ are key contributors to total interaction energy; (iii) terminal free carboxylate of Val411 and side chain carboxylate of Asp410 play an important role for the strong binding of the γC peptidic ligand; thus, for effective adhesion of fibrinogen to $\alpha_{IIb}\beta_3$ two free carboxylate groups at the end of the ligand are necessary; (iv) Asp224A, Asn215B, Asp159A and Lys125B of $\alpha_{IIb}\beta_3$ are the most important amino acid residues for binding of the C-terminal octapeptide part of fibrinogen; and (v) both the KQAGDV and KQRGDV peptidic sequences are structurally and chemically adopted to bind effectively $\alpha_{IIb}\beta_3$. The reason why some peptides with the AGD or RGD motif did not bind to $\alpha_{IIb}\beta_3$ is in structural and chemical nature of the C-terminal amino acid residue (X) in the AGDX or RGDX sequence rather than the AGD (or RGD) structure itself (e.g., AGDV or AGDF bind to $\alpha_{IIb}\beta_3$ while AGDC or AGDY not) (Kloczewiak et al. 1989).

From the X-ray structures of $\alpha_{IIb}\beta_3$ with the non-peptidic tirofiban and the L-739758 ligand it is evident that these antagonists mimic interactions of arginine and aspartic acid residues of the RGD motif of the peptidic ligands (contacts of tirofiban and L-739758 ligand with Asp224A and Mg^{2+} ion). Other hidden interactions were revealed by the FMO-PIEDA calculations in this work. As it was for the peptides, the MIDAS Mg^{2+} ion, the ADMIDAS Ca^{2+} ion, the LIMBS Ca^{2+} ion, Asp224A, Asn215B, Tyr122B, Lys125B and Tyr190A of $\alpha_{IIb}\beta_3$ are the most important contributors to total $\Delta E_{int(L:R)}$ for the $\alpha_{IIb}\beta_3$ complexes with the antagonists. In conclusion, new synthetically developed antagonists of $\alpha_{IIb}\beta_3$ should mimic not only the interactions of the RGD motif but also the interactions of the backbone of a longer peptidic sequence (RGDV or AGDV) with the focus on the interactions of the antagonists with the ADMIDAS Ca^{2+} ion.

The FMO-PIEDA calculations of the complexes of $\alpha_{IIb}\beta_3$ with the poly(L-lactic acid) chain indicate that a terminal carboxylate or a free carboxylate on the PLA surface are essential to mimic the adhesion process of the RGD-binding integrins. The PLA ester groups themselves

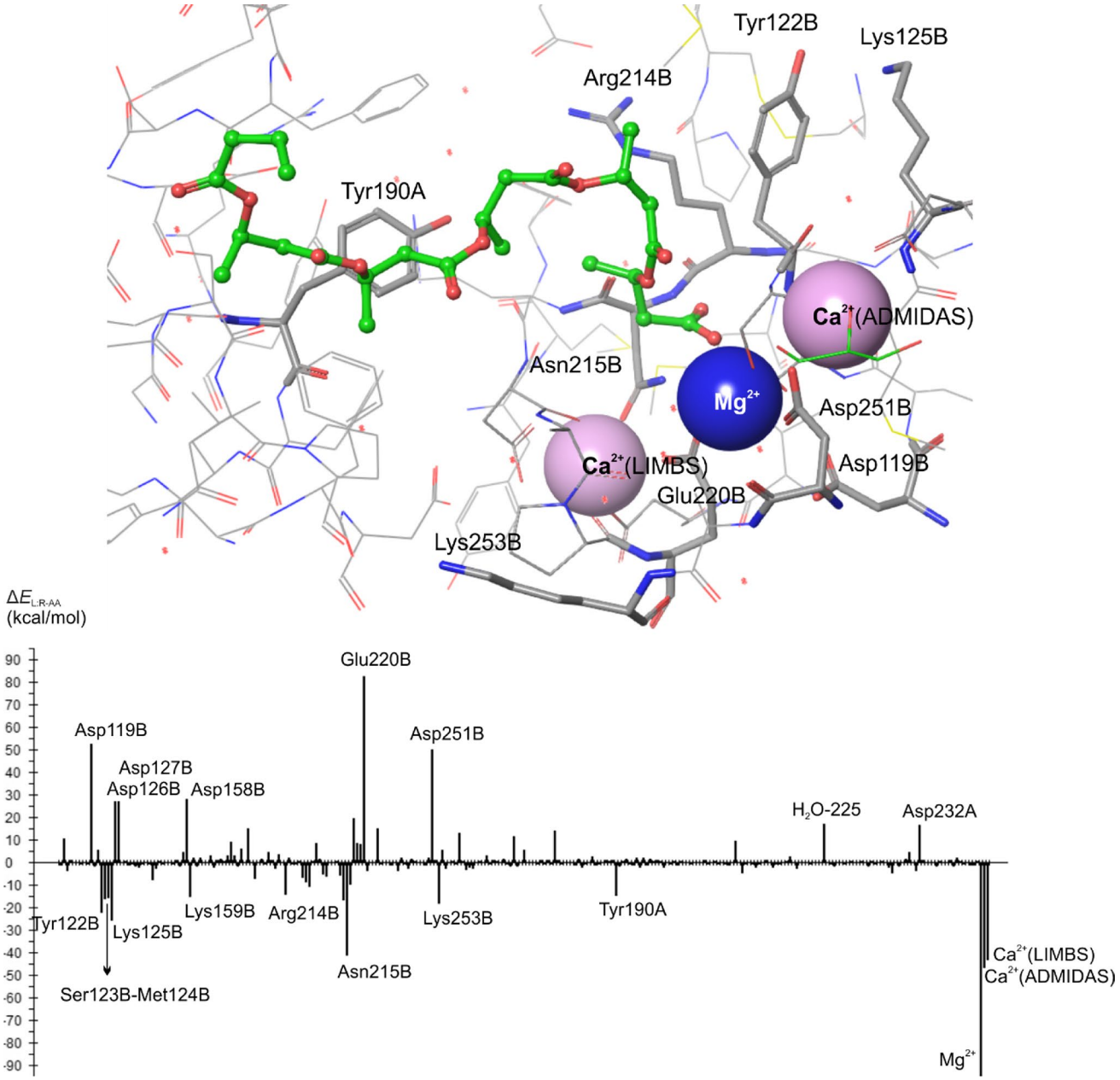

Fig. 12 FMO-PIEDA interaction energies ($\Delta E_{L:R\text{-}AA}$, in kcal mol^{-1}) between the PLA-01 ligand (PLA-COO$^-$) and the amino acid residues of $\alpha_{IIb}\beta_3$ calculated at the ab initio MP2/6-31G(d) level. The attraction terms of $\Delta E_{int(L:R)}$ present $\Delta E_{L:R\text{-}AA}$ with the negative values, while repulsion terms are with the positive values. The amino acid residues with the most significant $\Delta E_{L:R\text{-}AA}$ are visualized (tube representation, gray) as well as the PLA-01 ligand (ball-and-stick representation, green)

are not chemically so appropriate ligands for interactions with either Mg^{2+} and Ca^{2+} ions or amino acid residues at the ligand-binding site of $\alpha_{IIb}\beta_3$. In general, the adhesion of PLA surface on a cell may be more efficient when free carboxylates are available on polymer surfaces in repeated intervals.

Methodology

Structural models and molecular docking. The X-ray structures (Springer et al. 2008) of $\alpha_{IIb}\beta_3$ integrin with bound ligands (an octapeptide with the GAKQAGDV sequence, PDB ID: 2VDP (Springer et al. 2007b); a heptapeptide with the AKQRGDV sequence, PDB ID: 2VDR (Springer et al. 2007a); a cyclic peptide eptifibatide with the (HR)CCPWGDG sequence, PDB ID: 2VDN

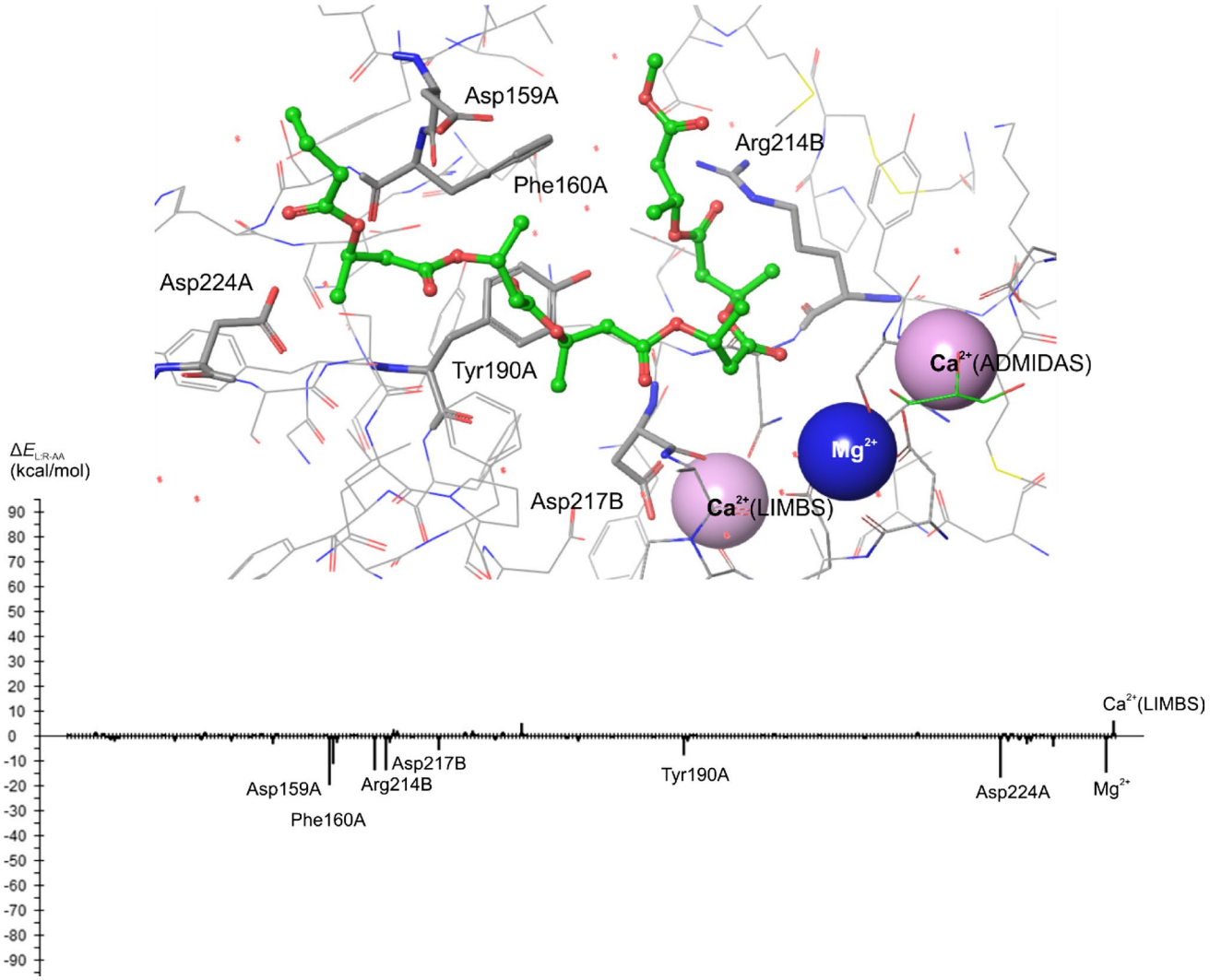

Fig. 13 FMO-PIEDA interaction energies ($\Delta E_{\text{L:R-AA}}$, in kcal mol^{-1}) between the PLA-03 (PLA-$COOCH_3$) ligand and the amino acid residues of $\alpha_{IIb}\beta_3$ calculated at the ab initio MP2/6-31G(d) level. The attraction terms of $\Delta E_{\text{int(L:R)}}$ present $\Delta E_{\text{L:R-AA}}$ with the negative values, while repulsion terms are with the positive values. The amino acid residues with the most significant $\Delta E_{\text{L:R-AA}}$ are visualized (tube representation, gray) as well as the bound PLA-03 ligand (ball-and-stick representation, green)

(Springer et al. 2007c); peptidomimetic tirofiban, PDB ID: 2VDM (Springer et al. 2007e) and the L-739758 ligand; PDB ID: 2VC2 (Springer et al. 2007d)) were used as 3-D structural models for QM/MM geometry optimizations and subsequent FMO-PIEDA calculations. The complex integrin $\alpha_{IIb}\beta_3$:poly(L-lactic acid) $(C_3H_4O_2)_{n=7}$ was built based on the X-ray structure of $\alpha_{IIb}\beta_3$ with the octapeptide with the AGD motif, PDB ID: 2VDP (Springer et al. 2007b)). The peptide and most water molecules were removed and a PLA chain was added to the ligand-binding site using of molecular docking. PLA was docked either in a charged form (with free terminal carboxylate, PLA-COO^-) or in a neutral form (with terminal methyl ester group, PLA-$COOCH_3$). Then, two bound conformations of PLA-COO^- in $\alpha_{IIb}\beta_3$ (PLA-01 and PLA-02) and one of the PLA-$COOCH_3$ (PLA-03) were selected based on a docking score for subsequent QM/MM and FMO-PIEDA calculations. The conformations PLA-01 and PLA-02 mimic the binding of a terminal C-region of fibrinogen to $\alpha_{IIb}\beta_3$ (Fig. 3). In these conformations terminal carboxylate of PLA was predicted to coordinate with the MIDAS Mg^{2+} ion. In the case of PLA-03 the docked chain mimics the binding of a non-terminal region of a peptidic ligand along a ligand-binding groove and MIDAS (Fig. 3).

Molecular docking was performed with the GLIDE program, version 7.0 (Friesner et al. 2004), of the Schrödinger package. For prediction of protonation states of the amino acid residues of $\alpha_{IIb}\beta_3$, the Propka version 2 empirical program (Li et al. 2005; Bas et al. 2008) was used (pH = 7.4). The receptor box with a size of $39 \times 39 \times 39$ Å was centered at the Mg^{2+} ion at MIDAS of $\alpha_{IIb}\beta_3$ using

OPLS2005 partial atomic charges (Kaminski et al. 2001). Flexible docking in standard (SP) precision was used. The potential for nonpolar parts of the ligands was softened by scaling the Van der Waals radii by a factor of 0.8 for atoms of the ligands with partial atomic charges less than specified cutoff of 0.15. For 10 ligand poses with the best docking score the post-docking minimization was performed.

QM/MM geometry optimizations. For the protein complexes ($\alpha_{IIb}\beta_3$:ligand), geometry optimizations at the QM/MM level were applied (BP86/LACVP*:OPLS2005) (Becke 1988; Wadt and Hay 1985; Kaminski et al. 2001) using the QSite (Murphy et al. 2000) program of the Schrödinger package. The QM part (more than 280 atoms) of the system included Mg^{2+} ion, Ca^{2+} ions and their coordinated ligands (amino acid residues and water molecules). The rest of the molecular system was calculated at the MM level described by the OPLS2005 force field (Kaminski et al. 2001). The QM/MM methodology (an additive scheme) with hydrogen caps on boundary QM atoms was used. Between the QM and MM regions, electrostatic treatment using Gaussian charge distributions was employed. The piperidine and carboxylate groups of tirofiban and the L-739758 ligand were modeled in ionized forms (as depicted in Fig. 2) according to the pK_a Propka calculations (Li et al. 2005; Bas et al. 2008).

FMO-PIEDA calculations. For the protein:ligand complexes, the two-body FMO method together with the pair interaction energy decomposition analysis (PIEDA) was used (Kitaura et al. 1999; Fedorov and Kitaura 2009; Fedorov et al. 2012). In FMO method, a biomolecular system is partitioned into fragments (with a fragment size—one amino acid residue). For modeling of the covalently bounded amino acids, the hybrid orbital projection operator (HOP) technique was applied. In the case of the peptidic ligands, the following two types of the fractioning were used in the FMO calculations: (i) the peptidic ligand was one large fragment consisted of all amino acid residues (i.e., for the octapeptide ligand with the AGD motif the fragment consists of 8 amino acid residues. The results are compiled in Table 1 and Figs. 4, 5, 6, 7, 8, 9, 12, 13); and (ii) the peptidic ligand was fragmented into separate amino acid residues according to a default FMO fragmentation technique with the shifted backbone definition (results in Table 2)(Sladek and Fedorov 2022). The QM/MM optimized structures of complexes ($\alpha_{IIb}\beta_3$:ligand) were reduced to ligand-binding site clusters consisted of more than 260 structural fragments (amino acid residues, Mg^{2+} and Ca^{2+} ions, structural water molecules and ligand. The cluster includes amino acid residues which are positioned in radius of 18 Å around Mg^{2+} ion. Detailed information about amino acid fragments can be found in pdb files included in ESI). The Facio program was used to prepare inputs for the FMO calculations (Suenaga 2008). The second-order Møller–Plesset theory (MP2) (Møller and Plesset 1934; Frisch et al. 1990) and density functional theory (DFT) wBP97X-D method (Becke 1997) with Grimme's empirical dispersion correction (Grimme 2006) were used with the 6-31G(d) basis and the conductor-like polarizable continuum model (C-PCM (PCM < 1 >, keywords IFMO = -1, IEF = -10, SOLVNT = WATER) (Fedorov 2019). The Gamess package (Barca et al. 2020; Schmidt et al. 1993) [version 30 June 2021 (R1), linux version] was employed. The pair interactions between the two structural fragments of the molecular system were predicted within the electrostatic potential of the surroundings. In our case the interactions between the fragments of the ligand (L) and the fragments of the receptor (R) were predicted. The FMO-PIEDA method separates the interaction energy into physically interpretable terms (1):

$$\Delta E_{L:R}^{int} = \Delta E_{L:R}^{els} + + \Delta E_{L:R}^{ct-mix} + \Delta E_{L:R}^{exch} + \Delta E_{L:R}^{disp} + \Delta G_{L:R}^{sol} \quad (1)$$

The electrostatic energy $\Delta E_{L:R}{}^{els}$ presents Coulomb-like interactions between the fragments. $\Delta E_{L:R}{}^{ct-mix}$ approximates polarization which originates from the charge transfer and the mixing part. The exchange energy $\Delta E_{L:R}{}^{exch}$ grows for fermion particles, the electrons and answers for the Pauli repulsion of electrons between the fragments. Dispersion energy $\Delta E_{L:R}{}^{disp}$ arises from fluctuations of dipoles on the fragments due to electron correlation. $\Delta G_{R:L}{}^{sol}$ is solute–solvent solvation free energy. FMO-PIEDA was successfully used in various proteins complexes (Lim et al. 2019; Sogawa et al. 2020; Anan et al. 2019; Sladek et al. 2017, 2018; Takaya et al. 2020; Kalník et al. 2023; Mironov et al. 2022).

To better understand a role of amino acid residues of the peptidic ligands with AGD and RGD motifs in the integrin-binding process and compare differences in an interaction pattern, the peptides with the GAKQAGDV and AKQRGDV sequences, and eptifibatide were divided into amino acid fragments [Ligand, L-AA(n)] in similar manner as amino acids of αIIbβ3 [Receptor, R-AA(m)]. Then, interaction energies between the ligand and the receptor will be marked as $\Delta E_{L\text{-}AA}(n)$ with total $\Delta E_{int(L:R)}$:

$$\Delta E_{int(L:R)} = \Delta E_{L-AA:R}(1) + \Delta E_{L-AA:R}(2) + \ldots + \Delta E_{L-AA:R}(n) \quad (2)$$

where $n = 8$ is for the GAKQAGDV sequence, $n = 7$ is for the AKQRGDV sequence and $n = 6$ is for eptifibatide. Then, the FMO-PIEDA analysis was also performed for a fragmentation scheme with the ligand as one structural fragment (Ligand, L) to see roles of amino acid residues of $\alpha_{IIb}\beta_3$ [Receptor, R-AA(m)] on the ligand binding. Then, interaction energies between the ligand and the receptor will be marked as $\Delta E_{L:R\text{-}AA}(m)$ with total $\Delta E_{int(L:R)}$:

$$\Delta E_{\mathrm{int(L:R)}} = \Delta E_{\mathrm{L:R-AA}}(1) + \Delta E_{\mathrm{L:R-AA}}(2) + \ldots + \Delta E_{\mathrm{L:R-AA}}(\mathrm{m}) \quad (3)$$

where m is number of amino acid fragments of the receptor $\alpha_{\mathrm{IIb}}\beta_3$. This FMO-PIEDA scheme was applied for all ligands calculated in this work.

Supplementary Information The online version contains supplementary material available at https://doi.org/10.1007/s11696-023-02910-4.

Acknowledgements This work was supported by the project implementation CEMBAM (Centre for Medical Bio-Additive Manufacturing and Research, ITMS2014+: 313011V358 supported by the Operational Programme Integrated Infrastructure funded by the European Regional Development Fund). Vladimir Sladek, PhD, is gratefully acknowledged for helpful discussions and careful reading of the manuscript.

Funding Open access funding provided by The Ministry of Education, Science, Research and Sport of the Slovak Republic in cooperation with Centre for Scientific and Technical Information of the Slovak Republic.

Declarations

Conflicts of interest There are no conflicts to declare.

References

Anan R, Nakamura T, Shimamura K, Matsushita Y, Ohyama T, Kurita N (2019) Change in binding states between catabolite activating protein and DNA induced by ligand-binding: molecular dynamics and ab initio fragment molecular orbital calculations. J Mol Model 25:192. https://doi.org/10.1007/s00894-019-4087-3

Arnaout MA, Mahalingam B, Xiong JP (2005) Integrin structure, allostery, and bidirectional signaling. Annu Rev Cell Dev Biol 21:381–410. https://doi.org/10.1146/annurev.cellbio.21.090704.151217

Barca GMJ, Bertoni C, Carrington L, Datta D, De Silva N, Deustua JE, Fedorov DG, Gour JR, Gunina AO, Guidez E, Harville T, Irle S, Ivanic J, Kowalski K, Leang SS, Li H, Li W, Lutz JJ, Magoulas I, Mato J, Mironov V, Nakata H, Pham BQ, Piecuch P, Poole D, Pruitt SR, Rendell AP, Roskop LB, Ruedenberg K, Sattasathuchana T, Schmidt MW, Shen J, Slipchenko L, Sosonkina M, Sundriyal V, Tiwari A, Vallejo JLG, Westheimer B, Wloch M, Xu P, Zahariev F, Gordon MS (2020) Recent developments in the general atomic and molecular electronic structure system. J Chem Phys 152:154102. https://doi.org/10.1063/5.0005188

Bas DC, Rogers DM, Jensen JH (2008) Very fast prediction and rationalization of pK(a) values for protein-ligand complexes. Proteins: Struct Funct, Bioinf 73:765–783. https://doi.org/10.1002/Prot.22102

Becke AD (1988) Density-functional exchange-energy approximation with correct asymptotic-behavior. Phys Rev A 38:3098–3100. https://doi.org/10.1103/physreva.38.3098

Becke AD (1997) Density-functional thermochemistry.5. Systematic optimization of exchange-correlation functionals. J Chem Phys 107:8554–8560. https://doi.org/10.1063/1.475007

Bidone TC, Polley A, Jin J, Driscoll T, Iwamoto DV, Calderwood DA, Schwartz MA, Voth GA (2019) Coarse-grained simulation of full-length integrin activation. Biophys J 116:1000–1010. https://doi.org/10.1016/j.bpj.2019.02.011

Campbell ID, Humphries MJ (2011) Integrin structure, activation, and interactions. Cold Spring Harb Perspect Biol 3:a004994. https://doi.org/10.1101/cshperspect.a004994

Chen W, Lou J, Hsin J, Schulten K, Harvey SC, Zhu C (2011) Molecular dynamics simulations of forced unbending of integrin αVβ3. PLoS Comput Biol 7:e1001086. https://doi.org/10.1371/journal.pcbi.1001086

Chothia C, Jones E (1997) The molecular structure of cell adhesion molecules. Ann Rev Biochem 66:823–862. https://doi.org/10.1146/annurev.biochem.66.1.823

Craig D, Gao M, Schulten K, Vogel V (2004) Structural Insights into how the MIDAS ion stabilizes integrin binding to an RGD peptide under force. Structure 12:2049–2058. https://doi.org/10.1016/j.str.2004.09.009

Dhavalikar P, Robinson A, Lan Z, Jenkins D, Chwatko M, Salhadar K, Jose A, Kar R, Shoga E, Kannapiran A, Cosgriff-Hernandez E (2020) Review of integrin-targeting biomaterials in tissue engineering. Adv Healthc Mater 9:2000795. https://doi.org/10.1002/adhm.202000795

Dong X, Hudson NE, Lu C, Springer TA (2014) Structural determinants of integrin β-subunit specificity for latent TGF-β. Nat Struct Mol Biol 21:1091–1096. https://doi.org/10.1038/nsmb.2905

Fedorov DG, Kitaura K (2009) Theoretical background of the fragment molecular orbital (FMO) method and its implementation in Gamess. In: Fedorov DG, Kitaura K (eds) The Fragnemt Molecular Orbital Method—Practical Applications to Large Molecular Systems. CRC Press, Taylor and Francis Group, pp 5–36

Fedorov DG, Kitaura K, Li H, Jensen JH, Gordon MS (2006) The polarizable continuum model (PCM) interfaced with the fragment molecular orbital method (FMO). J Comput Chem 27:976–985. https://doi.org/10.1002/jcc.20406

Fedorov DG, Nagata T, Kitaura K (2012) Exploring chemistry with the fragment molecular orbital method. Phys Chem Chem Phys 14(21):7562–7577. https://doi.org/10.1039/c2cp23784a

Friesner RA, Banks JL, Murphy RB, Halgren TA, Klicic JJ, Mainz DT, Repasky MP, Knoll EH, Shelley M, Perry JK, Shaw DE, Francis P, Shenkin PS (2004) Glide: a new approach for rapid, accurate docking and scoring. 1. Method and assessment of docking accuracy. J Med Chem 47:1739–1749. https://doi.org/10.1021/Jm0306430

Frisch MJ, Headgordon M, Pople JA (1990) A direct Mp2 gradient-method. Chem Phys Lett 166:275–280. https://doi.org/10.1016/0009-2614(90)80029-D

Gaillard T, Dejaegere A, Stote RH (2009) Dynamics of β3 integrin I-like and hybrid domains: Insight from simulations on the mechanism of transition between open and closed forms. Proteins 76:977–994. https://doi.org/10.1002/prot.22404

Ghitti M, Spitaleri A, Valentinis B, Mari S, Asperti C, Traversari C, Rizzardi GP, Musco G (2012) Molecular dynamics reveal that isoDGR-containing cyclopeptides are true αVβ3 antagonists unable to promote integrin allostery and activation. Angew Chem Int Ed 51(31):7702–7705. https://doi.org/10.1002/anie.201202032

Grimme S (2006) Semiempirical GGA-type density functional constructed with a long-range dispersion correction. J Comput Chem 27:1787–1799. https://doi.org/10.1002/jcc.20495

Harjunpää H, Asens ML, Guenther C, Fagerholm SC (2019) Cell adhesion molecules and their roles and regulation in the immune and tumor microenvironment. Front Immunol 10:1078. https://doi.org/10.3389/fimmu.2019.01078

Huang J, Li X, Shi X, Zhu M, Wang J, Huang S, Huang X, Wang H, Li L, Deng H, Zhou Y, Mao J, Long Z, Ma Z, Ye W, Pan J, Xi X, Jin J (2019) Platelet integrin alphaIIbbeta3: signal transduction, regulation, and its therapeutic targeting. J Hematol Oncol 12:26. https://doi.org/10.1186/s13045-019-0709-6

Humphries MJ (2000) Integrin structure. Biochem Soc Trans 28:311–339

Humphries JD, Byron A, Humphries MJ (2006) Integrin ligands at a glance. J Cell Sci 119:3901–3903. https://doi.org/10.1242/jcs.03098

Hynes RO (2002) Integrins: bidirectional, allosteric signaling machines. Cell 110:673–687. https://doi.org/10.1016/s0092-8674(02)00971-6

Kalník M, Šesták S, Kóňa J, Bella M, Poláková M (2023) Two-step continuous-flow synthesis of 6-membered cyclic iodonium salts via anodic oxidation. Beilstein J Org Chem 19:282–293. https://doi.org/10.3762/bjoc.19.24

Kaminski GA, Friesner RA, Tirado-Rives J, Jorgensen WL (2001) Evaluation and reparametrization of the OPLS-AA force field for proteins via comparison with accurate quantum chemical calculations on peptides. J Phys Chem B 105:6474–6487. https://doi.org/10.1021/jp003919d

Kapp TG, Rechenmacher F, Neubauer S, Maltsev OV, Cavalcanti-Adam EA, Zarka R, Reuning U, Notni J, Wester HJ, Mas-Moruno C, Spatz J, Geiger B, Kessler H (2017) A comprehensive evaluation of the activity and selectivity profile of ligands for RGD-binding integrins. Sci Rep 7:39805. https://doi.org/10.1038/srep39805

Kim TG, Park TG (2006) Biomimicking extracellular matrix: cell adhesive RGD peptide modified electrospun poly(D, L-lactic-co-glycolic acid) nanofiber mesh. Tissue Eng 12:221–233. https://doi.org/10.1089/ten.2006.12.221

Kitaura K, Ikeo E, Asada T, Nakano T, Uebayasi M (1999) Fragment molecular orbital method: an approximate computational method for large molecules. Chem Phys Lett 313:701–706. https://doi.org/10.1016/S0009-2614(99)00874-X

Kloczewiak M, Timmons S, Bednarek MA, Sakon M, Hawiger J (1989) Platelet receptor recognition domain on the γ chain of human fibrinogen and its synthetic peptide analogues. Biochemistry 28:2915–2919. https://doi.org/10.1021/bi00433a025

Kulke M, Langel W (2020) Molecular dynamics simulations to the bidirectional adhesion signaling pathway of integrin αVβ3. Proteins 88:679–688. https://doi.org/10.1002/prot.25849

Li H, Robertson AD, Jensen JH (2005) Very fast empirical prediction and rationalization of protein pK(a) values. Proteins: Struct Funct, Bioinf 61:704–721. https://doi.org/10.1002/Prot.20660

Lim H, Chun J, Jin X, Kim J, Yoon J, No KT (2019) Investigation of protein-protein interactions and hot spot region between PD-1 and PD-L1 by fragment molecular orbital method. Sci Rep 9:16727. https://doi.org/10.1038/s41598-019-53216-z

Luo BH, Carman CV, Springer TA (2007) Structural basis of integrin regulation and signaling. Annu Rev Immunol 25:619–647. https://doi.org/10.1146/annurev.immunol.25.022106.141618

Mehrbod M, Trisno S, Mofrad MRK (2013) On the activation of integrin αIIbβ3: outside-in and inside-out pathways. Biophys J 105:1304–1315. https://doi.org/10.1016/j.bpj.2013.07.055

Mironov V, Shchugoreva IA, Artyushenko PV, Morozov D, Borbone N, Oliviero G, Zamay TN, Moryachkov RV, Kolovskaya OS, Lukyanenko KA, Song YL, Merkuleva IA, Zabluda VN, Peters G, Koroleva LS, Veprintsev DV, Glazyrin YE, Volosnikova EA, Belenkaya SV, Esina TI, Isaeva AA, Nesmeyanova VS, Shanshin DV, Berlina AN, Komova NS, Svetlichnyi VA, Silnikov VN, Shcherbakov DN, Zamay GS, Zamay SS, Smolyarova T, Tikhonova EP, Chen KHC, Jeng US, Condorelli G, Franciscis V, Groenhof G, Yang CY, Moskovsky AA, Fedorov DG, Tomilin FN, Tan WH, Alexeev Y, Berezovski MV, Kichkailo AS (2022) Structure- and interaction-based design of anti-SARS-CoV-2 aptamers. Chem Eur J 28:e202104481. https://doi.org/10.1002/chem.202104481

Møller C, Plesset MS (1934) Note on an approximation treatment for many-electron systems. Phys Rev 46:618–622. https://doi.org/10.1103/PhysRev.46.618

Murcia M, Jirouskova M, Li J, Coller BS, Filizola M (2008) Functional and computational studies of the ligand-associated metal binding site of β3 integrins. Proteins 71:1779–1791. https://doi.org/10.1002/prot.21859

Murphy RB, Philipp DM, Friesner RA (2000) A mixed quantum mechanics/molecular mechanics (QM/MM) method for large-scale modeling of chemistry in protein environments. J Comput Chem 21:1442–1457. https://doi.org/10.1002/1096-987x(200012)21:16%3c1442::Aid-Jcc3%3e3.0.Co;2-O

Puklin-Faucher E, Vogel V (2009) Integrin activation dynamics between the RGD-binding site and the headpiece hinge. J Biol Chem 284:36557–33656. https://doi.org/10.1074/jbc.M109.041194

Puklin-Faucher E, Gao M, Schulten K, Vogel V (2006) How the headpiece hinge angle is opened: new insights into the dynamics of integrin activation. J Cell Biol 175:349–360. https://doi.org/10.1083/jcb.200602071

Ruggeri ZM, Houghten RA, Russell SR, Zimmerman TS (1986) Inhibition of platelet-function with synthetic peptides designed to be high-affinity antagonists of fibrinogen binding to platelets. Proc Natl Acad Sci USA 83:5708–5712. https://doi.org/10.1073/pnas.83.15.5708

Schmidt MW, Baldridge KK, Boatz JA, Elbert ST, Gordon MS, Jensen JH, Koseki S, Matsunaga N, Nguyen KA, Su SJ, Windus TL, Dupuis M, Montgomery JA (1993) General atomic and molecular electronic-structure system. J Comput Chem 14:1347–1363. https://doi.org/10.1002/jcc.540141112

Shekaran A, García AJ (2011) Extracellular matrix-mimetic adhesive biomaterials for bone repair. J Biomed Mater Res A 96:261–272. https://doi.org/10.1002/jbm.a.32979

Sladek V, Fedorov DG (2022) The importance of charge transfer and solvent screening in the interactions of backbones and functional groups in amino acid residues and nucleotides. Int J Mol Sci 23:13514. https://doi.org/10.3390/ijms232113514

Sladek V, Kóňa J, Tokiwa H (2017) In silico analysis of interaction pattern switching in ligand …receptor binding in Golgi alpha-mannosidase II induced by the protonated states of inhibitors. Phys Chem Chem Phys 19:12527–12537. https://doi.org/10.1039/c7cp01200d

Sladek V, Tokiwa H, Shimano H, Shigeta Y (2018) Protein residue networks from energetic and geometric data: Are they identical? J Chem Theory Comput 14:6623–6631. https://doi.org/10.1021/acs.jctc.8b00733

Sogawa H, Sato R, Suzuki K, Tomioka S, Shinzato T, Karpov P, Shulga S, Blume Y, Kurita N (2020) Binding sites of Zantrin inhibitors to the bacterial cell division protein FtsZ: molecular docking and ab initio molecular orbital calculations. Chem Phys 530:110603. https://doi.org/10.1016/j.chemphys.2019.110603

Spitaleri A, Mari S, Curnis F, Traversari C, Longhi R, Bordignon C, Corti A, Rizzardi GP, Musco G (2008) Structural basis for the interaction of isoDGR with the RGD-binding site of αVβ3 integrin. J Biol Chem 283(28):19757–19768. https://doi.org/10.1074/jbc.M710273200

Spitaleri A, Ghitti M, Mari S, Alberici L, Traversari C, Rizzardi GP, Musco G (2011) Use of metadynamics in the design of isoDGR-based αVβ3 antagonists to fine-tune the conformational ensemble. Angew Chem Int Ed 50:1832–1836. https://doi.org/10.1002/anie.201007091

Springer TA, Wang JH (2004) The three dimensional structure of integrins and their ligands, and conformational regulation of cell adhesion. Adv Protein Chem 68:29–63. https://doi.org/10.1016/S0065-3233(04)68002-8

Springer TTA, Zhu J, Xiao T (2007a) Integrin αIIbβ3 headpiece bound to a chimeric fibrinogen gamma chain peptide LGGAKQRGDV. PDB. https://doi.org/10.2210/pdb2212VDR/pdb

Springer TA, Zhu J, Xiao T (2007b) Integrin αIIbβ3 headpiece bound to fibrinogen gamma chain peptide LGGAKQAGDV. PDB. https://doi.org/10.2210/pdb2212VDP/pdb

Springer TA, Zhu J, Xiao T (2007c) Re-refinement of integrin αIIbβ3 headpiece bound to antagonist eptifibatide. PDB. https://doi.org/10.2210/pdb2212VDN/pdb

Springer TA, Zhu J, Xiao T (2007d) Re-refinement of integrin αIIbβ3 headpiece bound to antagonist L-739758. PDB. https://doi.org/10.2210/pdb2212VC2212/pdb

Springer TA, Zhu J, Xiao T (2007e) Re-refinement of integrin αIIbβ3 headpiece bound to antagonist tirofiban. PDB. https://doi.org/10.2210/pdb2212VDM/pdb

Springer TA, Zhu J, Xiao T (2008) Structural basis for distinctive recognition of fibrinogen γC peptide by the platelet integrin αIIbβ3. J Cell Biol 182:791–800. https://doi.org/10.1083/jcb.200801146

Suenaga M (2008) Development of GUI for GAMESS / FMO calculation. J Comput Chem-Japan 7:33–54. https://doi.org/10.2477/jccj.H1920

Suzuki S, Ikada Y (2010) Medical applications. In: Auras R, Lim LT, Selke SEM, Tsuji H (eds) Poly(Lactic Acid): Synthesis, Structures, Properties, Processing, and Applications. Wiley, pp 445–456. https://doi.org/10.1002/9780470649848

Takaya D, Niwa H, Mikuni J, Nakamura K, Handa N, Tanaka A, Yokoyama S, Honma T (2020) Protein ligand interaction analysis against new CaMKK2 inhibitors by use of X-ray crystallography and the fragment molecular orbital (FMO) method. J Mol Graph Model 99:107599. https://doi.org/10.1016/j.jmgm.2020.107599

Timmons S, Bednarek MA, Kloczewiak M, Hawiger J (1989) Antiplatelet hybrid peptides analogous to receptor recognition domains on γ-chain and α-chain of human-fibrinogen. Biochemistry 28:2919–2923. https://doi.org/10.1021/Bi00433a026

Tvaroška I, Kozmon S, Kóňa J (2023) Molecular modeling insights into the structure and behavior of integrins: a review. Cells 12:324–368. https://doi.org/10.3390/cells12020324

Wadt WR, Hay PJ (1985) Abinitio effective core potentials for molecular calculations—Potentials for main group elements Na to Bi. J Chem Phys 82:284–298. https://doi.org/10.1063/1.448800

Wang L, Pan D, Yan Q, Song Y (2017) Activation mechanisms of αVβ3 integrin by binding to fibronectin: a computational study. Protein Sci 26:1124–1137. https://doi.org/10.1002/pro.3163

Xiao T, Takagi J, Coller BS, Wang JH, Springer TA (2004) Structural basis for allostery in integrins and binding to fibrinogen-mimetic therapeutics. Nature 432:59–67. https://doi.org/10.1038/nature02976

Xiong JP, Stehle T, Zhang R, Joachimiak A, Frech M, Goodman SL, Arnaout MA (2002) Crystal structure of the extracellular segment of integrin αVβ3 in complex with an Arg-Gly-Asp ligand. Science 296:151–155. https://doi.org/10.1126/science.1069040

Yang Z, Kollman JM, Pandi L, Doolittle RF (2001) Crystal structure of native chicken fibrinogen at 2.7 A resolution. Biochemistry 40:12515–12523. https://doi.org/10.1021/bi011394p

Zhao J, Santino F, Giacomini D, Gentilucci L (2020) Integrin-targeting peptides for the design of functional cell-responsive biomaterials. Biomedicines 8:307. https://doi.org/10.3390/biomedicines8090307

Zheng YJ, Leftheris K (2020) Insights into protein-ligand interactions in integrin complexes: advances in structure determinations. J Med Chem 63:5675–5696. https://doi.org/10.1021/acs.jmedchem.9b01869

Zhu J, Luo BH, Xiao T, Zhang C, Nishida N, Springer TA (2008) Structure of a complete integrin ectodomain in a physiologic resting state and activation and deactivation by applied forces. Mol Cell 32:849–861. https://doi.org/10.1016/j.molcel.2008.11.018

Zhu J, Zhu J, Negri A, Provasi D, Filizola M, Coller BS, Springer TA (2010) Closed headpiece of integrin αIIbβ3 and its complex with an αIIbβ3-specific antagonist that does not induce opening. Blood 116:5050–5059. https://doi.org/10.1182/blood-2010-04-281154

Zhu JQ, Zhu JH, Springer TA (2013) Complete integrin headpiece opening in eight steps. J Cell Biol 201:1053–1068. https://doi.org/10.1083/jcb.201212037